PHAT XX. AGB Stars and Other Cool Giants in M31 Star Clusters

Availability:
This version is available at: 20.500.11767/122277 since: 2021-04-08T11:50:29Z

Publisher:

Terms of use:

Testo definito dall'ateneo relativo alle clausole di concessione d'uso

note finali coverpage

(Article begins on next page)

10 May 2024

PHAT XX. AGB Stars and Other Cool Giants in M31 Star Clusters

Léo Girardi[1] , Martha L. Boyer[2] , L. Clifton Johnson[3] , Julianne J. Dalcanton[4] , Philip Rosenfield[5] , Anil C. Seth[6] ,
Evan D. Skillman[7] , Daniel R. Weisz[8] , Benjamin F. Williams[4] , Antara Raaghavi Bhattacharya[9,21] , Alessandro Bressan[10] ,
Nelson Caldwell[11] , Yang Chen[12] , Andrew E. Dolphin[13,14] , Morgan Fouesneau[15] , Steven Goldman[2] ,
Puragra Guhathakurta[16] , Paola Marigo[12] , Sagnick Mukherjee[16,17] , Giada Pastorelli[2] , Amanda Quirk[16] ,
Monika Soraisam[18,19] , and Michele Trabucchi[12,20]

[1] Osservatorio Astronomico di Padova—INAF, Vicolo dell'Osservatorio 5, I-35122 Padova, Italy; leo.girardi@inaf.it
[2] Space Telescope Science Institute, 3700 San Martin Drive, Baltimore, MD 21218, USA
[3] Department of Physics and Astronomy, Northwestern University, 2145 Sheridan Road, Evanston, IL 60208, USA
[4] Department of Astronomy, University of Washington, Box 351580, Seattle, WA 98195, USA
[5] Eureka Scientific, Inc., 2452 Delmer Street, Oakland, CA 94602, USA
[6] Department of Physics and Astronomy, University of Utah, Salt Lake City, UT 84112, USA
[7] Minnesota Institute for Astrophysics, University of Minnesota, 116 Church St. SE, Minneapolis, MN 55455, USA
[8] Department of Astronomy, University of California, 501 Campbell Hall #3411, Berkeley, CA 94720-3411, USA
[9] Navy Children School, Mumbai, India
[10] SISSA, via Bonomea 365, I-34136 Trieste, Italy
[11] Harvard-Smithsonian Center for Astrophysics, 60 Garden Street, Cambridge, MA 02138, USA
[12] Dipartimento di Fisica e Astronomia Galileo Galilei, Università di Padova, Vicolo dell'Osservatorio 3, I-35122 Padova, Italy
[13] Raytheon, 1151 E. Hermans Road, Tucson, AZ 85706, USA
[14] Steward Observatory, University of Arizona, 933 North Cherry Avenue, Tucson, AZ 85721, USA
[15] Max-Planck-Institut für Astronomie, Königstuhl 17, D-69117 Heidelberg, Germany
[16] UCO/Lick Observatory, University of California Santa Cruz, 1156 High Street, Santa Cruz, CA 95064, USA
[17] Department of Physics, Presidency University, Kolkata, India
[18] National Center for Supercomputing Applications, University of Illinois at Urbana-Champaign, Urbana, IL 61801, USA
[19] Department of Astronomy, University of Illinois at Urbana-Champaign, Urbana, IL 61801, USA
[20] Department of Astronomy, University of Geneva, Ch. des Maillettes 51, 1290 Versoix, Switzerland

Abstract

The presence of asymptotic giant branch (AGB) stars in clusters provides key constraints for stellar models, as has been demonstrated with historical data from the Magellanic Clouds. In this work, we look for candidate AGB stars in M31 star clusters from the Panchromatic Hubble Andromeda Treasury survey. Our photometric criteria selects stars brighter than the tip of the red giant branch, which includes the bulk of the thermally pulsing AGB stars as well as early-AGB stars and other luminous cool giants expected in young stellar populations (e.g., massive red supergiants, and intermediate-mass red helium-burning stars). The AGB stars can be differentiated, a posteriori, using the ages already estimated for our cluster sample. 937 candidates are found within the cluster aperture radii, half ($\sim$450) of which are very likely cluster members. Cross-matching with additional databases reveals two carbon stars and 10 secure variables among them. The field-corrected age distribution reveals the presence of young supergiants peaking at ages smaller than 10^8 yr, followed by a long tail of AGB stars extending up to the oldest possible ages. This long tail reveals the general decrease in the numbers of AGB stars from initial values of $\sim$50 $\times$ $10^{-6}M_\odot^{-1}$ at 10^8 yr down to $\sim$5 $\times$ $10^{-6}M_\odot^{-1}$ at 10^{10} yr. Theoretical models of near-solar metallicity reproduce this general trend, although with localized discrepancies over some age intervals, whose origin is not yet identified. The entire catalog is released together with finding charts to facilitate follow-up studies.

1. Introduction

Stellar clusters with known ages and metallicities allow one to securely anchor the initial masses of stars evolving within them. This approach is particularly valuable for stars that are intrinsically challenging to model, due to their rapid evolution and complex interior physics. Asymptotic giant branch (AGB) stars, in particular, have benefited from systematic studies of their properties in stellar clusters, although such studies have been limited due to their rarity in any individual cluster.

There are at least 124 AGB stars belonging to 31 Magellanic Clouds' (MC) clusters (Frogel et al. 1990). Some remarkable cases are NGC 419 in the Small MC (SMC) and NGC 1846 in the Large MC (LMC), with $\sim$20 likely AGB members each, which are probably the places in the known universe with the highest spatial concentration of resolved carbon stars.

During the dawn of near-infrared (NIR) astronomy, in the 1970s and 1980s, observations of these MC clusters have been crucial to the development of a general picture about the evolution of AGB stars, especially regarding their final thermally pulsing (TP-AGB) phase where the processes of third dredge-up, hot-bottom-burning, long-period variability and dust-driven mass loss take place (see Lattanzio & Wood 2004; Herwig 2005; Höfner & Olofsson 2018, for reviews). By the time of Frogel et al. (1990), some basic facts were already clear, for instance

---

1. The initially more massive stars, found in the younger star clusters, reach higher luminosities along the TP-AGB than less massive stars, found in the oldest clusters.
2. Luminous giants rich in C-bearing molecules (hereafter C stars) are generated only inside a limited range of initial masses, in contrast with the O-rich giants (generally known as M giants).
3. The TP-AGB lifetimes, limited to luminosities above the tip of the RGB of intermediate-age and old populations, are of the order of a few Myr at most.

Subsequent works used these cluster data to derive more quantitative constraints on several aspects of the AGB evolution, including those on the C- and M-type lifetimes (Girardi & Marigo 2007), on the fraction of the integrated light contributed by the TP-AGB phase (Maraston 2005; Pessev et al. 2008; Noël et al. 2013), on the dust emission by the mass-losing, extreme-AGB stars (van Loon et al. 2005), and on the connections between mass loss, long-period variability, and surface chemical composition (Lebzelter et al. 2008; Kamath et al. 2010, 2012).

Yet despite their richness, relative proximity, little reddening, and nearly constant distance, the MC clusters are far from being the ideal sample for the study of AGB stars. They do not uniformly cover the age interval in which AGB stars are produced (Marigo et al. 1996), and span a limited range of metallicities. Moreover, even for the richest MC clusters, there are significant stochastic fluctuations in the numbers of evolved stars, which is reflected in all quantities derived from them, including their integrated colors (Santos & Frogel 1997).

In principle, some of these problems can be alleviated by grouping several clusters into a few age bins (as done by e.g., Maraston 2005; Girardi & Marigo 2007; Pessev et al. 2008; Noël et al. 2013). However, some of the quantitative constraints on the AGB evolution derived in this way have been questioned after the discovery of the "AGB boosting" effect at ages of ~1.6 Gyr (Girardi et al. 2013). In short, it happens that for a limited interval of ages the numbers of observed AGB stars in clusters (and all derived quantities) are not proportional to the AGB lifetime—and, unfortunately, most of the MC cluster data concentrates close to this age limit.

That said, it would be very important if other rich samples of AGB stars belonging to star clusters were available, so that the trends observed in the MCs could be checked and extended to a wider range of ages and metallicities. Star clusters in the Milky Way (MW) Galaxy are not that useful in this regard. Although many MW old globular clusters have a clear "early-AGB bump" along their red giant branches (RGBs; see e.g., Ferraro et al. 1999), they generally do not present many stars above the tip of the red giant branch (TRGB) that could be clearly assigned to the TP-AGB phase, with a few exceptions like 47 Tuc (Lebzelter & Wood 2005; McDonald et al. 2011a; Momany et al. 2012; Lebzelter et al. 2014) and ω Cen (Boyer et al. 2008; McDonald et al. 2009, 2011b). In many other cases the MW globular clusters host just a handful of candidate TP-AGB stars selected on the basis of their long-period variability (Lebzelter & Wood 2011). Nearby open clusters are in general too poorly populated to present even a single AGB star. Star clusters in other Local Group dwarf galaxies suffer from the same problems. Beyond the Local Group, there are many super-star clusters that probably contain many AGB stars each (e.g., Schweizer et al. 1996; Whitmore et al. 1999). They,

however, are not resolved into individual objects even when observed with the Hubble Space Telescope (HST).

The Andromeda (M31) and Triangulum (M33) galaxies are the obvious candidates to obviate such a situation. They are located at distances in which they are resolvable into stars by the HST, contain stellar populations of all ages (Ferguson et al. 2005; Brown et al. 2006; Javadi et al. 2011; Bernard et al. 2012, 2015; Lewis et al. 2015; Williams et al. 2017), and host hundreds of candidate star clusters (Galleti et al. 2004; Sarajedini & Mancone 2007; Peacock et al. 2010; San Roman et al. 2010; Johnson et al. 2012). Until recently, however, the necessary HST imaging was not available, beyond limited areas across these galaxies and for a few of its most conspicuous clusters (e.g., Williams & Hodge 2001; Caldwell et al. 2009). More critically, the available high-resolution imaging did not include the NIR, which is crucial for a clear identification of the TP-AGB stars.

For M31, the situation has radically changed with the Panchromatic Hubble Andromeda Treasury (PHAT; Dalcanton et al. 2012) survey, which collected UV, optical, and NIR imaging for about 1/3 of M31 disk, and most of its bulge. PHAT now includes 2753 star clusters identified through the citizen-scientists Andromeda Project[25] (AP; Johnson et al. 2015). They are a rich ground for searches of stars in relatively rapid phases of their evolution, as demonstrated by the identification of a number of Cepheids (Senchyna et al. 2015) and a planetary nebula (Davis et al. 2019) in them. It is also interesting to note that the PHAT mean spatial resolution (1 ACS/WFC pixel = 0.19 pc in the optical, 1 WFC3/IR pixel = 0.5 pc in the NIR) is similar to the resolution that was obtained from the ground for MC clusters ($1'' = 0.25$ pc for the LMC) at the dawn of NIR astronomy (Frogel et al. 1990 and references therein), and is still comparable to the resolution being obtained in present studies of the MCs in the NIR (e.g., Cioni et al. 2011).

In this paper, we provide a first list of AGB candidates in M31 star clusters, and discuss their reliability. We look for candidates at luminosities above the TRGB, which means that the sample may include multiple stellar types, including non-AGB stars at young ages (see discussion in Section 3), a combination of early-AGB and TP-AGB stars at intermediate-ages, then exclusively TP-AGB stars at ages older than ~3 Gyr. Throughout this work, we will use a generic "AGB" label to refer to the cases in which AGB stars (both early-AGB and TP-AGB) are likely present, and an even more generic "AGB candidate" to refer to the samples that may include a significant fraction of very young, non-AGB stars. Data and methods are described in Section 2. The properties of the derived sample are discussed in Section 3. A few conclusions are drawn in Section 4.

2. Data and Methods

2.1. PHAT Imaging and Photometry

The PHAT survey is extensively described in Dalcanton et al. (2012). Its extended, 0.5 deg²-wide footprint can be appreciated in Figure 1. The HST imaging was organized into 23 "bricks" of $6' \times 12'$ each, formed by 3×6 contiguous pointings (or "fields") of the Wide Field Camera 3 (WFC3)

---

[25] Indeed, between the metallicity values we plot in Figure 14, the total lifetimes of RSG phases change by factors of just ~10 % for a given mass.
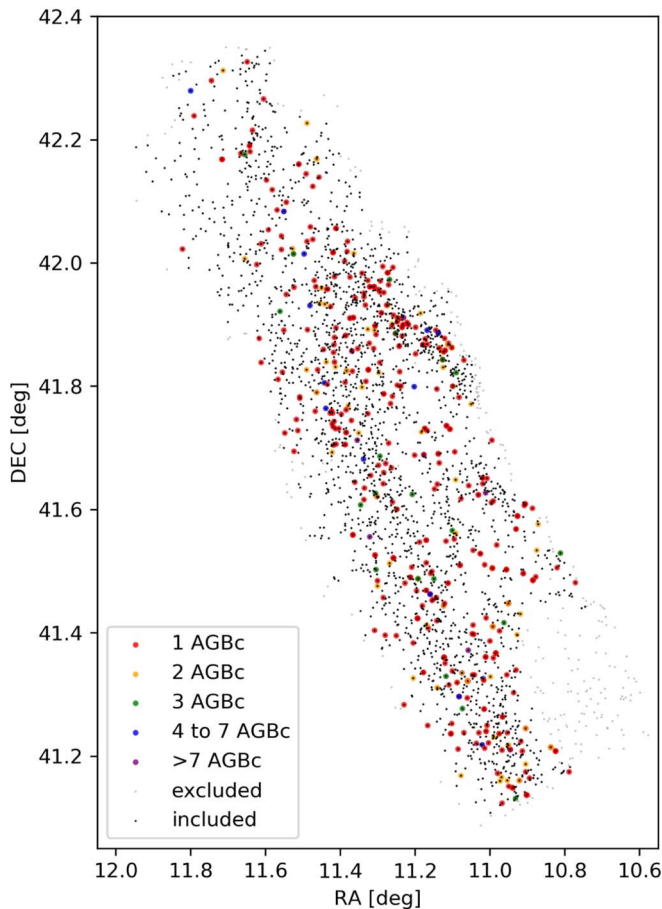[22] http://www.andromedaproject.org/

Figure 1. Sky distribution of PHAT star clusters from the AP catalog (small dots).The gray dots mark clusters excluded from our sample, either because they belong to the M31 bulge (at the bottom-right corner) or because they do not have NIR photometry. The remaining black dots are clusters searched for AGB stars. The colored circles mark the clusters where they are found, with their numbers per cluster as in the legend.

NIR channel. The same bricks were imaged in two ultraviolet bands with the WFC3 ultraviolet/optical (UVIS) channel, and at a separation of 6 months in the optical with the Advanced Camera for Surveys (ACS) Wide Field Channel (WFC). Williams et al. (2014) describe the complex work of aligning all the images and performing simultaneous 6-filter photometry in them. It resulted in photometric measurements for over 117 million stars in M31. The final catalog is available at the Mikulski Archive for Space Telescopes (MAST),[25] and contains several useful photometry quality flags.

The best photometry is obtained for the two optical filters of ACS/WFC, F475W and F814W, which present the most favorable combination of exposure time and spatial resolution. Indeed, in these filters the photometry reaches more than 3 mag below the red clump, except in the most crowded areas close to the M31 bulge. The WFC3/IR photometry in F110W and F160W is also of excellent quality, thanks to the lower level of crowding caused by the blue main-sequence stars at these wavelengths and by the use of simultaneous optical and IR photometry (Williams et al. 2014). The NIR photometry is generally limited to the upper RGB and above, but also extends to below the red clump in the outermost PHAT bricks.

---
[23] https://archive.stsci.edu/prepds/phat/

2.2. Cluster Catalogs

In this paper we use the AP cluster catalog from Johnson et al. (2015). It comprises the complete PHAT area as illustrated in Figure 1. It includes 2753 clusters identified by citizen scientists and later verified with the aid of the Year 1 catalog (a data set identified by professional astronomers, limited to four PHAT bricks plus two half-bricks, see Johnson et al. 2012) and with fake clusters inserted in the original images. Because the catalog is sorted with the highest fractions of users identifying clusters first, objects with smaller AP numbers correspond to clusters more evident to the eye—which usually means they are younger, more populous, and in M31 areas with a simpler foreground/background. Clusters in the AP catalog are also characterized by their central coordinates, and by their "aperture radii," R_{ap}, which mark the visible extent of the clusters. They are calculated using the median values of the individual cluster centers and radii measured by AP users.

From the AP catalog, we have excluded clusters without NIR imaging from PHAT, and 106 clusters belonging to the highly crowded bulge area (see Figure 12 in Johnson et al. 2015). We are then left with a sample of 2501 clusters. Physical parameters of the clusters have been determined in an homogeneous way by Johnson et al. (2015). The cluster ages include color–magnitude ages for younger clusters ($\lesssim$300 Myr) as presented in Johnson et al. (2016), and integrated-light estimates of the ages and masses using Fouesneau et al. (2014)'s method by Beerman (2015).

Given the way the AP catalog was built and the variety of cluster sizes, concentrations, and foreground/background across the M31 disk, there is no one-to-one relationship between R_{ap} and other commonly adopted cluster structural parameters such as the half-light radius, R_{eff}. But cluster-to-cluster estimates of R_{eff} based on radial profiles (Table 2 in Johnson et al. 2015), and extensive experiments with fake clusters added to PHAT images (their Table 6), indicate that R_{ap} is typically between 1 and 5 times larger than R_{eff}. Just 3% of the fake clusters presented by Johnson et al. (2015) turn out to have R_{ap} smaller than R_{eff}.

2.3. Candidate AGB Stars in PHAT

From the 6-filter photometry of low-surface-brightness areas, we build the NIR color–magnitude diagram (CMD) of Figure 2. The sample is limited to stars that satisfy the good star (GST) quality criterion for the photometry defined in Williams et al. (2014), in both NIR passbands. In short, the GST criterion is designed to eliminate objects strongly affected by blending, cosmic rays, or instrument artifacts. In the NIR filters, it consists in keeping only measurements for which the photometric pipeline (namely DOLPHOT; see Dolphin 2016) returned a signal-to-noise larger than 4, a sharpness-squared smaller than 0.15, and a crowding parameter smaller than 2.25 mag.

Figure 2 clearly shows the TRGB and the population of AGB stars immediately above it. To avoid the rich population of RGB stars, we select stars at least 0.1 mag brighter than the TRGB as measured in Figure 2, which translates into

$$F160W < 18.14 \text{ mag.} \tag{1}$$

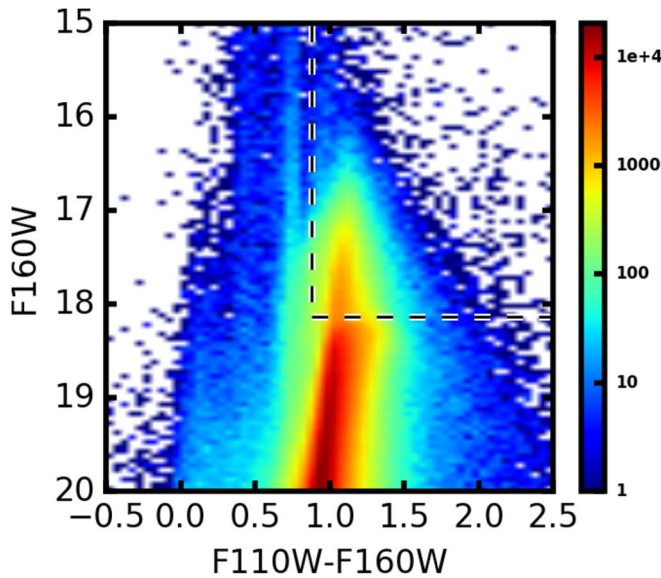In addition, we adopt a blue color cut designed to limit contamination by young red supergiants (RSGs) and

Figure 2. Field NIR CMD from the PHAT low-density regions (density of RGB stars with $18.5 < \mathrm{F160W} < 19.5$ smaller than 0.3 arcsec^{-2}, see Williams et al. 2014), illustrating the selection of AGB candidates in the region above and to the right of the dashed line. The selected stars are just red enough to avoid the vertical stripe of foreground low-mass main-sequence stars at $\mathrm{F110W} - \mathrm{F160W} \sim 0.7$ mag, and just bright enough to avoid the well-populated RGB region starting at $\mathrm{F160W} \gtrsim 18.2$ mag.

foreground dwarfs:

$$\mathrm{F110W} - \mathrm{F160W} > 0.88 \text{ mag.} \qquad (2)$$

We recall that the bulk of (essentially unreddened) foreground MW stars are located in a vertical sequence at $\mathrm{F110W} - \mathrm{F160W} = 0.7$ mag (Dalcanton et al. 2012; Williams et al. 2014), which is also evident in Figure 2.

Even with the above-mentioned color cut, a whole class of young luminous giants may still contaminate our list of AGB candidates. These include massive RSGs, and possibly also intermediate-mass red helium-burning stars, which are as bright as TP-AGB stars and which can become red enough (as a result of high metallicity or high reddening) to enter into our selection box (see Dalcanton et al. 2012). However, those contaminants belonging to star clusters might be avoided by simply eliminating the youngest clusters from our discussion, as we show later in Section 3. These selection criteria will also miss many of the so-called extreme-AGB stars, which are reddened and dimmed by several magnitudes in the NIR, owing to their own circumstellar dust shells. These stars will be fainter than the NIR TRGB, but will be discussed with their Spitzer IR photometry in a forthcoming paper (S. Goldman et al. 2020, in preparation).

We have explored similar criteria to select candidate AGB stars from the optical observations as well:

$$\begin{aligned} \mathrm{F814W} &< 0.09828(\mathrm{F475W}-\mathrm{F814W})^2 \\ &\quad - 0.3578(\mathrm{F475W}-\mathrm{F814W}) + 20.455 \end{aligned} \qquad (3)$$

$$\mathrm{F475W}-\mathrm{F814W} > 21.675 - 0.91875\,\mathrm{F814W}. \qquad (4)$$

However, this sample is less complete than the NIR one, and includes a significant number of "optical AGB candidates" which are actually far away from the region selected in the NIR CMD of Figure 2. A similar problem was recently uncovered by Boyer et al. (2019), who shows how NIR-bright M stars move to magnitudes fainter than the TRGB in the F814W

passband (see their Figure 6). Therefore, we exclude the optical criteria from our discussion.

Based on the NIR selection, we identify 255,671 candidate NIR AGB stars in the entire PHAT 6-filter catalog, which covers nearly 1/3 of the M31 disk. ~150,000 of these stars belong to the bulge area (mainly to Brick 1). This alone is an impressive statistic, to be compared to the ~61,000 and 8,500 candidate TP-AGBs identified in the LMC and SMC, respectively, using similar NIR criteria (Cioni et al. 2006a, 2006b; Boyer et al. 2011). The density of AGB candidate stars decreases nearly exponentially with galacto-centric radius. In addition, there is a strong concentration in the bulge, and some mild concentrations along the 10 kpc ring and the overdensity at 3.5 kpc identified by Davidge (2012). The ratio of AGB stars to RGB stars varies with radius, and is twice as high in the outer disk as in the inner disk. This is probably caused by a combination of the larger metallicities (expected shorter TP-AGB lifetimes) and larger fraction of older populations (again shorter TP-AGB lifetimes) in the inner M31 disk.

2.4. Matching AGB Stars and Clusters

The 255,671 AGB stars will be a mixture of numerous field-AGB stars and a smaller number that are true cluster members. We identify this latter population by looking at all possible AGB-cluster matches and looking for excesses above what is expected for a pure field-AGB population.

We cross-match our list of candidate AGB stars with the AP cluster catalog, initially keeping all candidates within a radius $R_{\mathrm{sc}} < 60''$ (225 pc) from the optically determined cluster centers, which results in over 615,000 AGB-cluster pairs. The top panel of Figure 3 shows the histogram of R_{sc} values of AGB-cluster pairs up to $10''$, together with the distribution of aperture radii, R_{ap}, for the clusters. We find that for all $R_{\mathrm{sc}} \gtrsim 4''$ the number of pairs increases linearly with R_{sc}, as expected from a sample dominated by random matches between clusters and uniformly distributed field stars. Figure 3, however, clearly shows that there is an excess of matches for $R_{\mathrm{sc}} < 2''$. The bulk of clusters in the AP catalog has aperture radii, R_{ap}, ranging from $1''$ to $2''$, as also shown in Figure 3. It becomes evident that there is an excess of AGB candidates observed at $R_{\mathrm{sc}} \lesssim R_{\mathrm{ap}}$, with respect to the numbers expected from a uniform distribution. By extending the line obtained for large R_{sc} toward the $R_{\mathrm{sc}} = 0$, $n(R_{\mathrm{sc}}) = 0$ limit (Figure 3, top panel), we can even determine that the excess of matches above this line amounts to 438 stars.

We repeat the exercise of measuring the excess, but using separations normalized by the size of the cluster, R_{ap}. The distribution of the $R_{\mathrm{sc}}/R_{\mathrm{ap}}$ ratio is shown in the bottom panel of Figure 3. A total of 937 AGB candidates are found at $R_{\mathrm{sc}}/R_{\mathrm{ap}} < 1$. This time we decide to measure the field stellar density in an annulus extending from 2 to 4 times R_{ap}. Extrapolation of the field stellar density down to the $R_{\mathrm{sc}}/R_{\mathrm{ap}} = 0$, $n(R_{\mathrm{sc}}/R_{\mathrm{ap}}) = 0$ limit reveals that the excess of AGB stars starts at $R_{\mathrm{sc}}/R_{\mathrm{ap}}$ values slightly below 1, although it becomes really evident only at $R_{\mathrm{sc}}/R_{\mathrm{ap}} < 0.6$. The excess amounts to 477 ± 10, which is about half of the number of TP-AGB stars observed at $R_{\mathrm{sc}}/R_{\mathrm{ap}} < 1$, and comparable to the number inferred from the analysis of R_{sc}.

We therefore infer that the AP clusters contain about 450 likely AGB members inside their R_{ap}, and about the same number of "field intruders." That said, it is nearly impossible to
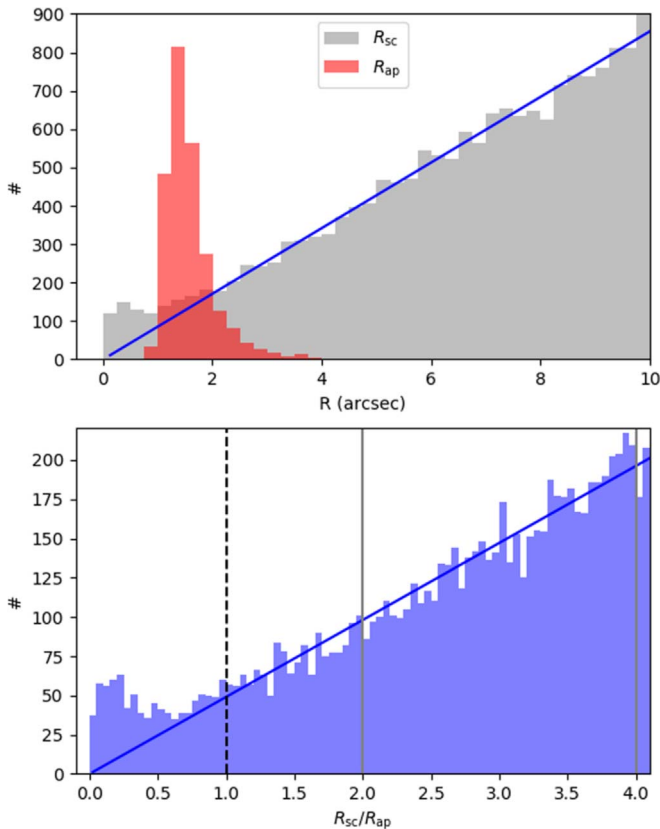
Figure 3. Top panel: distribution of separations between candidate AGB stars and cluster centers, R_{sc}, for the 2491 candidates found with separations smaller than $10''$ (gray histogram). The plotted line shows the linear distribution expected from random matches; its mean slope is derived from all stars with R_{sc} between $6''$ and $60''$. For comparison, the red histogram shows the distribution of cluster aperture radii R_{ap} in the AP catalog. Bottom panel: distribution of the ratio between separation and the aperture radius, R_{sc}/R_{ap}. The gray continuous vertical lines delimit the region used to estimate the mean field density, while the dashed line marks the upper limit adopted for building the present catalog.

say with certainty whether an individual AGB star in a cluster is a member or not. The approach to be followed must therefore be a statistical one, in which membership probabilities are assigned. In the discussion that follows, we adopt an inclusive criterion, considering all stars inside R_{ap} as possible cluster members.

Figures 4 and 5 illustrate a few "good cases" in which the association between candidate AGB stars and clusters appears evident, especially in the latter, for which candidates are multiple and could hardly result from field contamination or crowding. Figure 6 instead shows an example in which no AGB star was found inside R_{ap} despite the favorable conditions, plus a few somewhat dubious cases of association. There are many other situations in which the association between the AGB stars and the clusters—or even the AGB classification—could be questioned using either photometric or astrophysical arguments. In the following, we will discuss a few aspects that can help us to distinguish between likely and unlikely associations.

Before proceeding, however, we note that both the cluster centers (used to derive R_{sc}) and R_{ap} were measured from the optical images, and hence they are unlikely to be strongly affected by the presence of some very few NIR-bright

candidate AGB stars in their neighborhood. Indeed, this appears clear from the images in Figures 4–6.

2.5. Characterization of Crowding

An excess of bright NIR stars inside the cluster cores could well be caused by crowding (understood as photometric errors plus stellar blends), rather than by the presence of bright cluster members. Globular clusters in the MW provide good examples of crowding affecting the brightness of red giants in infrared passbands (see, e.g., Boyer et al. 2010). Fortunately, the work by Williams et al. (2014) allows us to make a first evaluation of these effects on our catalog.

The six filter photometry catalog from Williams et al. (2014) has a crowding parameter in each filter that characterizes how much brighter the star would have been had nearby stars not been fit simultaneously. For the F160W filter, this parameter is the `F160W_crowd` parameter in the databases, which we refer to here as $F160W_{crowd}$. Figure 7 shows the distribution of this parameter for the samples of candidate AGB stars both inside and outside clusters. Stars outside clusters ($R_{sc} > R_{ap}$) have $F160W_{crowd}$ typically constrained below 0.2 mag. Stars inside clusters present nearly the same distribution of crowding parameters but have an additional long tail of higher $F160W_{crowd}$ values, with 260 stars (27% of the sample) having $F160W_{crowd} > 0.2$ mag. This behavior is closely followed by $F110W_{crowd}$. This indicates that in-cluster crowding is probably affecting a good fraction of our sample. We have flagged in our catalogs the objects (265 out of 937) for which the sum of F160W and $F160W_{crowd}$ could put stars below the minimum magnitude for being classified as an AGB, that is $F160W + F160W_{crowd} > 18.1$ mag. One such example is the AGB star in AP 147, illustrated in Figure 6. In a similar way, we also flag 33 additional stars for which the "uncrowded color" would bee too blue, i.e., $F110W + F110W_{crowd} - F160W - F160W_{crowd} < 0.88$ mag. This is not a determinant criterion to exclude stars from our catalog, however, since the photometry was correctly done using all neighboring sources. This is just a flag to pinpoint objects where the photometry and AGB classification are possibly more affected by crowding, than usual.

To better characterize the level of crowding star-by-star, we can also employ the artificial stars tests performed by Williams et al. (2014, see their Section 5) on PHAT stacked images. They were performed for a few representative values of "RGB star densities," or ρ_{RGB}, intended as the number of stars of $18.5 <$ F160W < 19.5 per arcsec^2. Particularly relevant in the context of this paper are the "magnitude random errors and biases" for stars located very close to the TRGB, namely at F160W $= 18.24$ mag, which are plotted in the top panel of Figure 8. A magnitude bias < -0.1 mag could easily cause the numerous RGB stars present in the cluster and field to enter into the AGB area of the CMD. Similarly, a magnitude random error exceeding 0.1 mag would cause a sizeable fraction of these RGB stars to be randomly scattered in the same region.

The bottom panel of Figure 8 presents the distribution of stellar density of RGB stars with $18.5 <$ F160W < 19.5, ρ_{RGB}, for our candidate AGB stars in clusters, measured inside the R_{ap} of each cluster. Many clusters have a so scarcely populated RGB that this parameter turns out to be null, which essentially points to negligible crowding in the cluster core compared to the environment of typical field-AGB stars. More populous clusters have a significant number of RGB stars, but their ρ_{RGB}
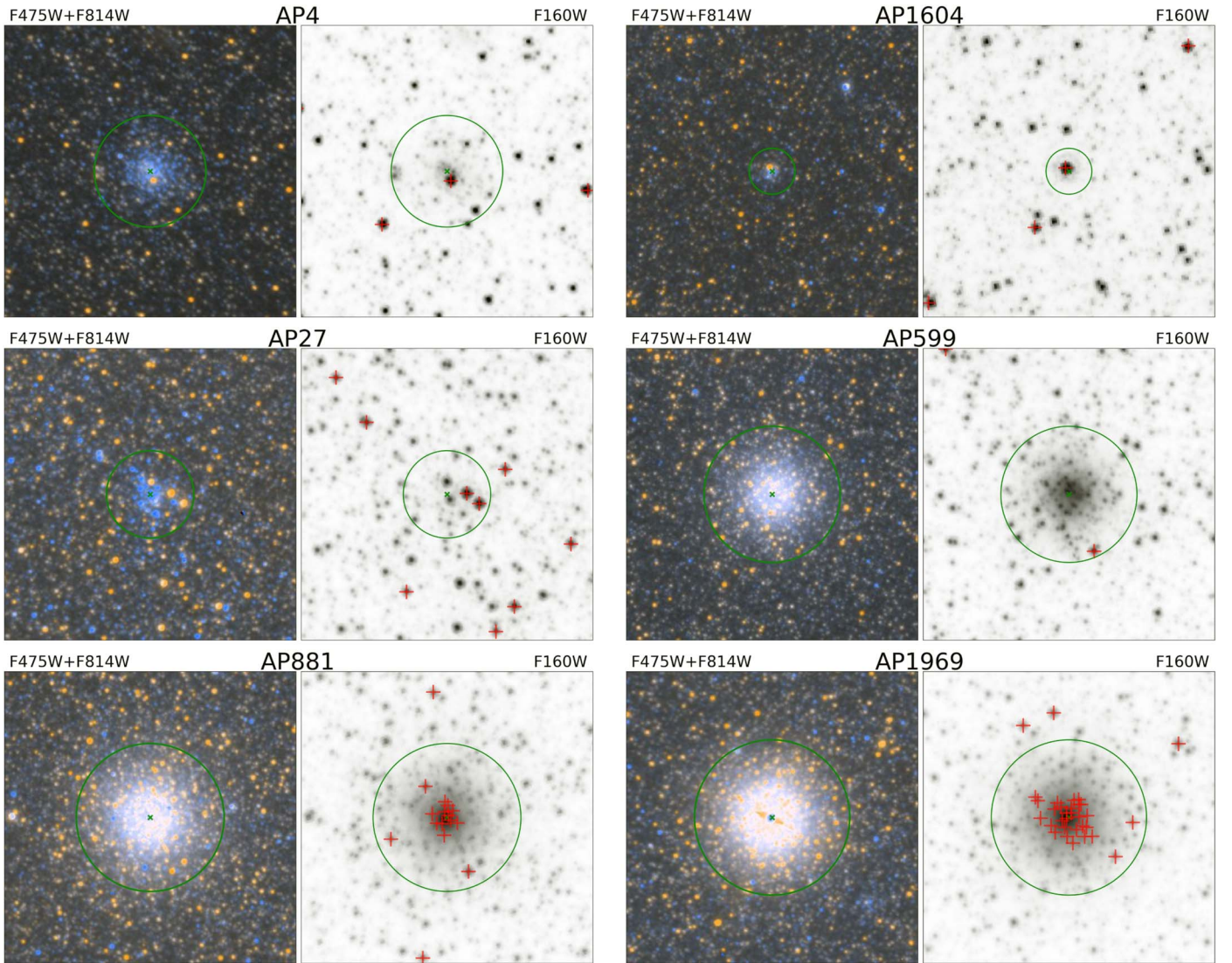
Figure 4. Examples of AP clusters containing AGB candidates. For each cluster, the left panel shows a false-color representation of the PHAT F475W+F814W optical images, which was used to find the clusters and derive their morphological parameters in Johnson et al. (2015), while the right panel shows the F160W image, whose photometry is crucial for identifying the AGB stars in this work. Images are centered on the cluster and have dimensions of $15'' \times 15''$ (or 5.7 pc $\times$ 5.7 pc), with North up and East left. In green we mark the cluster center and aperture radius R_{ap}, in red (in the F160W image only) all the candidate AGB stars in the area. Six examples are shown: AP 4 (the first entry in the catalog) and AP 1604 illustrate the almost-perfect superposition between intermediate-age clusters and lone, very bright and red AGB stars. We note the unusual compactness of AP 1604, which makes the association particularly compelling. AP 27 is a young cluster with two candidate AGB stars clearly standing out due to their NIR brightness; both are also the brightest red giants in the composite optical image. AP 599, AP 881, and AP 1969 represent a sequence of globular-like clusters of increasing central density and likely old age (see https://www.cfa.harvard.edu/oir/eg/m31clusters/phat). AP 599 (B201-G250) has a lone AGB candidate slightly off-center, despite sitting in a field in which AGB stars are actually rare. AP 881 (B218-G272) and AP 1969 (B225-G280) are old globular clusters with many bright red giants, 14 and 29 of which, respectively, are candidate AGB stars. It is clear that their center most candidates could be affected by crowding errors and even by blending of multiple NIR sources; however, the outermost sources inside R_{ap} are free from these problems, and likely cluster members.

never exceeds 1.1 arcsec^{-2}. At these maximum RGB densities, the magnitude bias turns out to be tiny (about ~ -0.006 mag), although the magnitude rms error (bottom panel of Figure 8) amounts to a very significant ~ 0.12 mag. Assuming a Gaussian distribution of magnitude errors, the faintest among our candidate AGB stars could actually be TRGB stars (or real AGB stars slightly fainter than the TRGB) which entered into the AGB selection region just because of the photometric scatter. However, we verified that this fraction is very small: just 55 AGB candidates (shown in Figure 8), or $\sim 6\%$ of the sample, have a F160W magnitude compatible with it being a TRGB star scattered upwards by one rms. These cases include

AGB candidates in dense globular clusters such as AP 1969 (B225-G280; Figure 4).

Overall, these estimates of the cluster densities and crowding errors are quite crude and subject to many uncertainties: few RGB stars per cluster, no real fitting of cluster density profile, no real estimate of the likelihood of RGB stars being scattered into the AGB region, etc. Moreover, it suffices to examine Figure 4 to conclude that proper estimates of the effect of crowding would require extensive—and time-consuming—experiments of artificial star tests using the actual cluster images, or fully synthetic cluster tests. For the moment, we limit ourselves to making our ρ_{RGB} estimates available in the final catalog, so that potential users can appreciate, with the
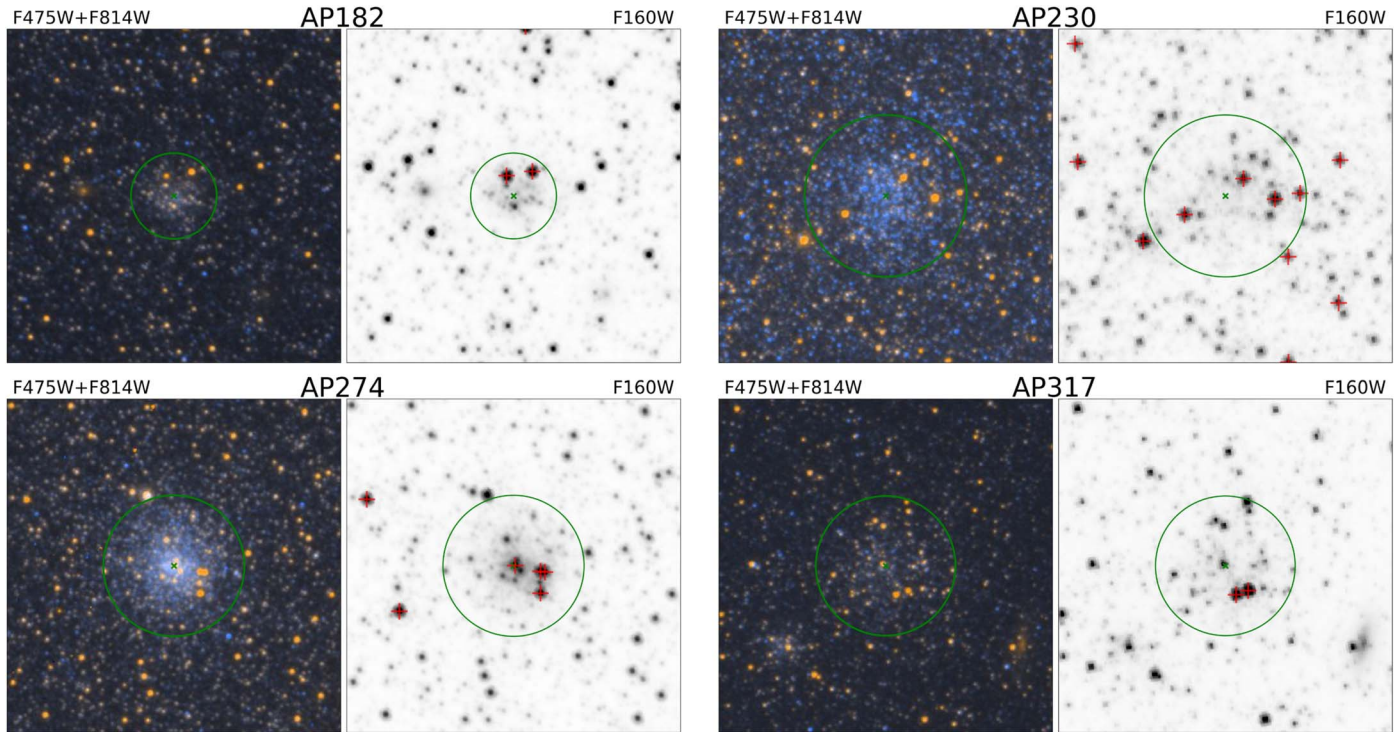
Figure 5. Same as in Figure 4, but now illustrating cases in which the association between stars and clusters is particularly compelling, thanks to the multiple AGB candidates on the cluster area, the uncrowded images, and the low field contamination.

help of Figure 8, the chances that AGB candidates in a particular cluster are significantly affected by crowding.

2.6. C/M Classification with WFC3/IR Medium-band Filters

We augment our catalog of cluster AGB candidates with estimates of their spectral subtypes where available.

First, we use results from Boyer et al. (2013, 2019), who performed an HST survey using WFC3/IR medium-band filters in 21 regions across the PHAT footprint, to classify their bright red giants as either C- or M-type. Their method uses the sensitivity of the filters F127M, F139M, and F153M to the presence of either $CN + C_2$ or H_2O absorption features in the NIR. We cross-match our sample of 937 candidate AGB stars in clusters with the complete Boyer et al. (2019) catalog. We find a total of 59 robust matches, for which the differences between the catalogs are smaller than $0\rlap{.}''04$ in position, and smaller than 0.017 mag in both F110W and F160W magnitudes. All of them are classified as M stars. The lack of C stars is this small sample is not surprising, given the remarkable scarcity of C stars in M31, especially in its innermost regions (Boyer et al. 2019). Indeed the average C/M ratio across the M31 disk amounts to just ~0.02.

2.7. Keck/DEIMOS Spectroscopy

As an extension of the Spectroscopic and Photometric Landscape of Andromeda's Stellar Halo survey (e.g., Guhathakurta et al. 2005, 2006; Gilbert et al. 2006), we used the Keck II 10 m telescope and DEIMOS spectrograph to obtain spectra of PHAT-selected star clusters and individual stars in the disk of M31 (Dorman et al. 2012, 2013, 2015; Quirk et al. 2019). The spectra fall into two categories: (1) low-resolution spectra obtained with the 600ZD grating that cover the approximate wavelength range 4500–9500 Å, and (2) medium-resolution

spectra obtained with the 1200G grating that cover the approximate wavelength range 6500–9000 Å. In the entire database, we find 24 unique spectroscopic matches with clusters hosting AGB candidates. Some examples of spectra are shown in Figure 9 along with the corresponding star cluster image and DEIMOS slit overlay. It is important to note that the FWHM of seeing during the spectroscopic observations was in the range $0\rlap{.}''5$–$0\rlap{.}''9$ (for reference, the width of the DEIMOS slit is $0\rlap{.}''8$) so these spectra are generally composite spectra of more than one bright cluster star. The TP-AGB star in the cluster AP 1018 turns out to be a carbon star; note the strong "W"-shaped CN spectral absorption feature at 7800–8200 Å. The remaining three spectra shown display a much weaker version of this same "W"–shaped CN spectral absorption feature, a feature that appears to be associated with evolved massive (5–10 $M_\odot$) stars (P. Guhathakurta et al. 2020, in preparation).

Clear signatures of carbon stars are found only in the clusters AP 1018 (see Figure 9) and AP 1508. These are low-mass clusters with very uncertain integrated-light ages, with 16%–84% confidence intervals for $\log(t/\mathrm{yr})$ being 8.9–9.8 and 8.1–9.5, respectively. These two cases add to the very limited list of C stars in metal-rich open clusters, presently consisting of just four candidates in the MW open clusters NGC 2477 (Catchpole & Feast 1973), NGC 2660 (Hartwick & Hesser 1973), NGC 7789 (Gaustad & Conti 1971), and Trumpler 5 (Kalinowski et al. 1974).

2.8. Variability

The $160'' \times 160''$ field of view of the WFC3/IR F110W and F160W images is the smallest of the cameras/modes used in the PHAT project, and this sets the step size of the brick-based tiling used in the survey. By contrast, the field of view of the ACS/WFC F475W and F814W images is $205'' \times 205''$ which
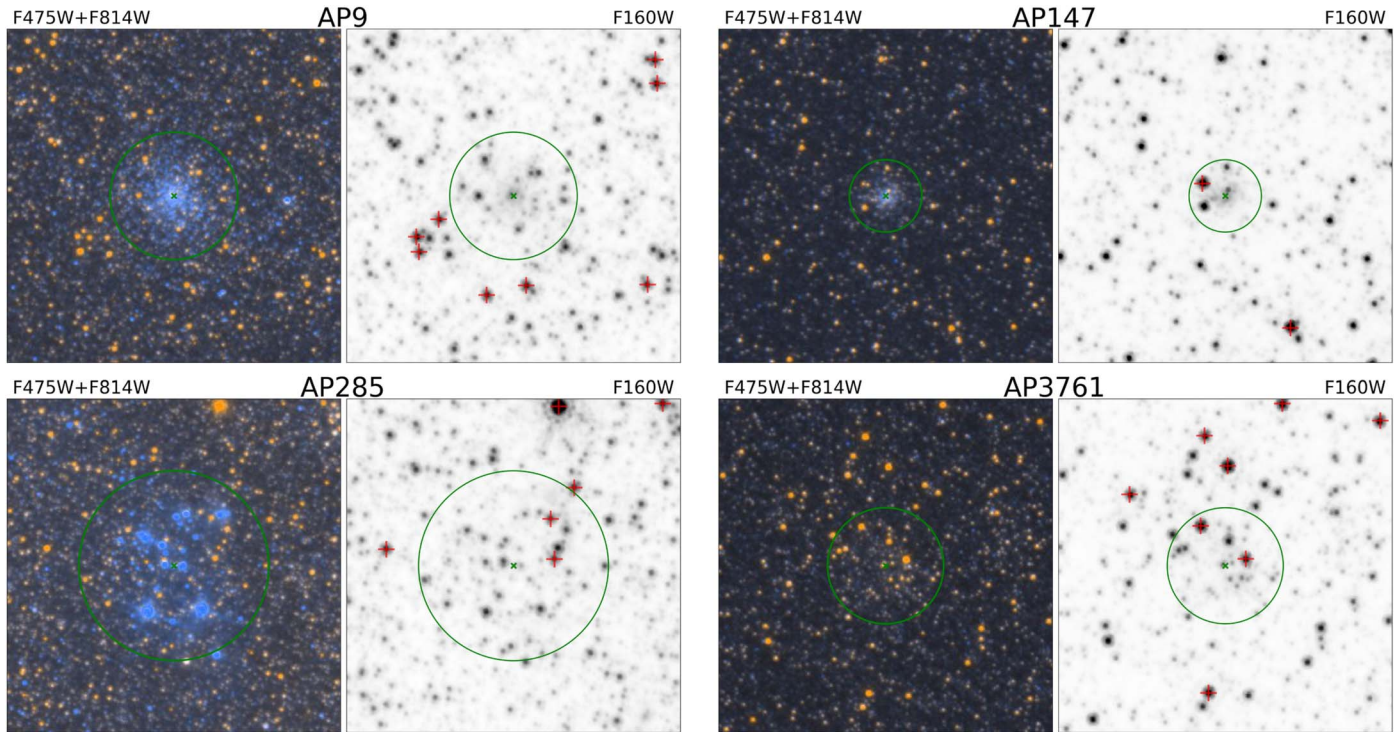
Figure 6. Same as in Figure 4, but now illustrating negative and potentially problematic results. First, we show AP 9 as an example of non-detection; this cluster is well populated and has the right age to contain AGB stars ($\log t/\mathrm{yr}$ between 8.6 and 9.1), but none is close enough to classify as a likely cluster member. AP 147 contains one candidate AGB with F160W = 18.111 mag, which is just slightly above the F160W limit we define. However, the optical images (which have a better resolution than the F160W one) indicate that the NIR source might be affected by the near-blending of two red giants. Although its $\mathrm{F160W_{crowd}}$ parameter is of just 0.048 mag, this introduces enough uncertainty in its NIR magnitude that this star could actually be fainter than the F160W magnitude limit we set for the AGB sample. AP 285 instead contains two bright NIR sources inside the cluster R_{ap} but it is probably too young ($\log t/\mathrm{yr}$ between 6.45 and 6.75) to contain genuine AGB stars. These are more likely reddened RSGs, or field-AGB stars falling inside the large R_{ap} of this cluster. Finally, AP 3761 has two candidate AGB stars but suffers from a more generic problem: clusters with high AP numbers tend to be fuzzier, less massive, and have badly defined limits, compared to those with low AP numbers. These uncertainties affect the estimates of the cluster center and R_{ap}, and hence the membership probabilities, ages, and mass estimates.
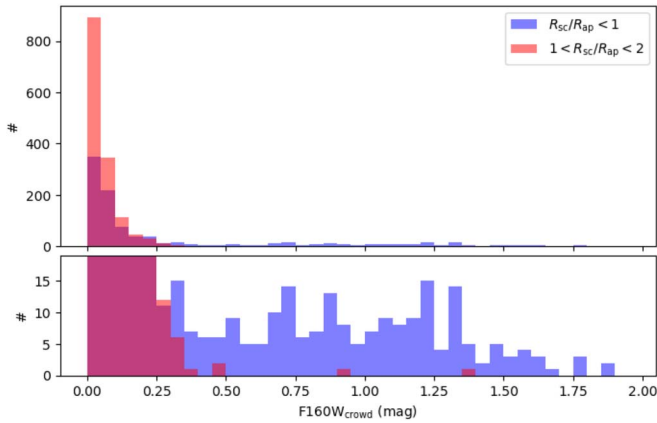

Figure 7. Top panel presents a histogram of the parameter $\mathrm{F160W_{crowd}}$ for candidate AGB stars both inside (blue) and immediately outside R_{ap} (red). The bulk of the distribution is located at $\mathrm{F160W_{crowd}} < 0.2$ mag, which overall points to a modest impact of crowding in the NIR photometry of the entire sample. The bottom panel zooms on the tail of large $\mathrm{F160W_{crowd}}$ values presented by the sample inside R_{ap}.

leads to significant overlap between adjacent pointings in these two filters. We have used time-resolved PHAT photometry (derived from constrained PSF fits to individual ACS exposures) in both F814W and F475W filters to search for variability among the AGB candidates that are located within star clusters in the overlap areas. For about 20% of them, the time baseline over which repeat F475W and F814W photometry is available is $\gtrsim 100$ days, which is comparable to the timescale on which AGB stars are expected to vary (Soraisam et al. 2020). The photometry time baseline for the remaining 80% of the stars is < 30 days, which is short enough that we do not expect to detect significant variability. These two subsamples of AGB stars are hereafter referred to as the long time baseline (LTB) and short time baseline (STB) subsamples, respectively.

We use a chi-squared statistic as a measure of variability compared to the mean magnitude, and compute its value using the photometric measurements for each of our AGB stars in both F814W and F475W filters. We also characterize an average systematic error (e.g., due to crowding or cosmic ray hits) in the photometric measurements using the STB AGB stars in the sample. We use the 95th percentile of the distribution of chi-squared values of the STB AGBs in both F814W and F475W filters as thresholds for variability. We find 20 LTB AGBs above these thresholds. To confirm that this variability is not affected by the presence of some other bright star/variable star nearby or the crowding of the cluster, we look at individual HST images (in both F814W and F475W). Of the 20 stars, we find 10 of them as secure variables. One evident example is presented in Figure 10. The other 10 stars are affected by the crowding of the clusters or bad quality exposures. The details of this analysis along with a population of all detected variables in PHAT clusters (including the non-
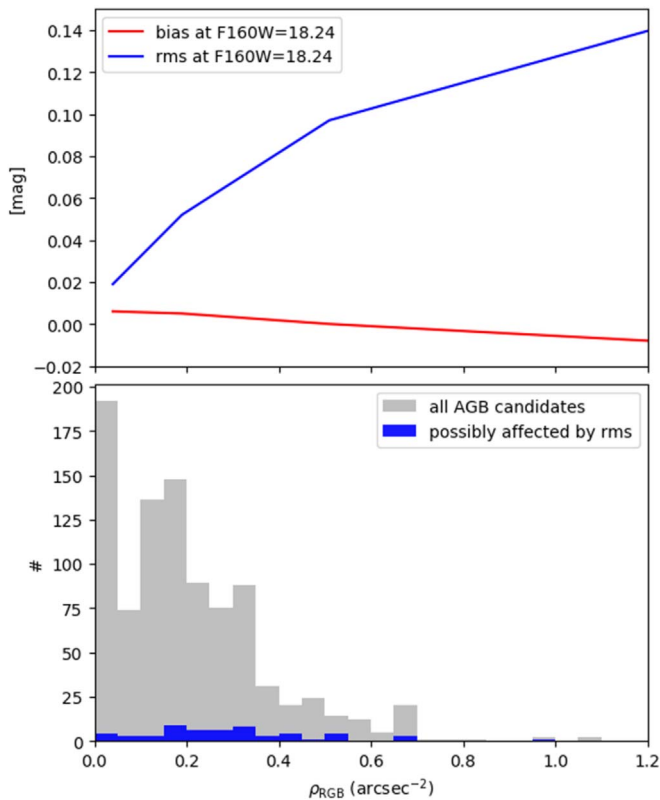
Figure 8. Top panel: the magnitude bias and rms error for stars at the TRGB (F160W = 18.24 mag), plotted over the interval of RGB densities relevant for the star clusters. The curves are determined by linear interpolation of the values determined by Williams et al. (2014) using artificial star tests of F160W = 18.0 mag and F160W = 18.5 mag. Bottom panel: the gray histogram shows the distribution of RGB densities for all 937 candidate AGB stars in clusters. The blue histogram shows the 55 stars whose magnitudes are compatible with a TRGB star being scattered upwards by the same amount as the rms. Similarly, we checked which AGB candidates could be stars at the TRGB moved into the AGB region by the photometric bias, but no such case was found.

AGB ones) will be published in S. Mukherjee et al. (2020, in preparation).

3. Sample Properties

AGB-cluster candidates are only expected to be real AGB stars for cluster ages larger than ~100 Myr. In younger clusters, post-He-burning stars do not develop a carbon–oxygen (or oxygen–neon in the case of the super-AGB stars) electron-degenerate core (Herwig 2005), and as a consequence have a much quicker evolution up to pre-supernova stages. Moreover, across the entire age range in which AGB stars appear, their numbers are expected to vary as a consequence of multiple processes (third dredge-up, hot-bottom-burning, carbon-star formation, onset of fundamental-mode high amplitude pulsation, dust-driven stellar winds, etc.) which occur with varying efficiency as a function of stellar mass and metallicity during the thermally pulsing phase (see e.g., Marigo & Girardi 2007). Revealing this sequence of AGB star frequency and properties as a function of stellar age (and mass), and possibly also of metallicity, is actually one of the best reasons to define samples of AGB stars in clusters, as in the present paper.

In this section, we attempt for a first interpretation of the data in terms of cluster ages, t. For a given age, the numbers of AGB

stars observed in clusters should also scale with the cluster total mass, M_{tot}, so we need to characterize both quantities before dealing with the AGB stars themselves.

3.1. Age and Mass Distributions of Clusters

We take the quantities t and M_{tot} derived by Fouesneau et al. (2014) and Beerman (2015) for the clusters in the AP catalog. More specifically, we use the pair of values that corresponds to their "best method," which derive either from fitting of isochrones in the case of clusters with a good-quality CMD, or from the the integrated optical magnitudes and colors when the CMD is deemed too uncertain. Out of the 2753 clusters in our initial catalog, 2736 have these quantities determined. CMD ages (from Johnson et al. 2016) are available for 1253 clusters, generally corresponding to the youngest part of the cluster sample.

Figure 11 shows the global properties of the clusters used in this work, in the $\log t$ versus $\log M_{tot}$ plane. As can be noticed, the sample includes large numbers of young and intermediate-age low-mass clusters (with $M_{tot} \lesssim 10^4 M_\odot$, see top-left panel), but the total mass of the cluster sample is instead concentrated at ages older than a few Gyr (see top-right panel), which include clusters with masses in excess of $M_{tot} \gtrsim 10^5 M_\odot$. There are also clear trends in the mean sky area, πR_{ap}^2, covered by clusters of different age and mass, as shown in the bottom-left panel. Clusters with larger M_{tot} tend to cover larger areas, but this also happens for very young clusters, with ages $t \lesssim 10^7$ yr. Together with the distribution of numbers of cluster (top-left panel), these trends give origin to the distribution of total area depicted in the bottom-right panel.

Whenever necessary, we use the estimated 1σ errors in age and mass as being half the difference between the 16% and 84% percentiles in their probability density functions in logarithmic space. We recall that the age determinations coming from integrated photometry, by their own nature, are uncertain, with typical errors amounting to ~0.2 dex. But again, this situation compares well with the situation for the MC clusters in the 1980s, for which the best ages and mass estimates were coming from integrated photometry rather than from their (very noisy, at the time) CMDs.

Before proceeding, we should define the most suitable age binning for the clusters in our analysis. In Figure 11, and in the following, we choose a bin width of 0.3 dex in $\log t$ (or a factor of 2 in linear age) primarily because narrower bins would decrease the numbers of AGB candidates to values below ~10 at some age intervals, producing significantly noisier histograms for the quantities we are going to measure. ~80 % of the clusters with age determinations have 1σ errors smaller than this bin width.

3.2. Age Distribution of AGB Candidates

AGB candidates inside R_{ap} are attributed the same age t as their hosting cluster, and associated to a stellar population parent mass equal to M_{tot}. The top-left panel of Figure 12 shows the distribution of their numbers in the t versus M_{tot} plane. This distribution somewhat reflects the distribution of cluster total masses already shown in Figure 11. More remarkable is the fact that AGB candidates are concentrated in the age interval between $\log(t/\mathrm{yr}) = 8.1$ and 9.3. Comparison with the numbers of clusters in Figure 11 reveals that the
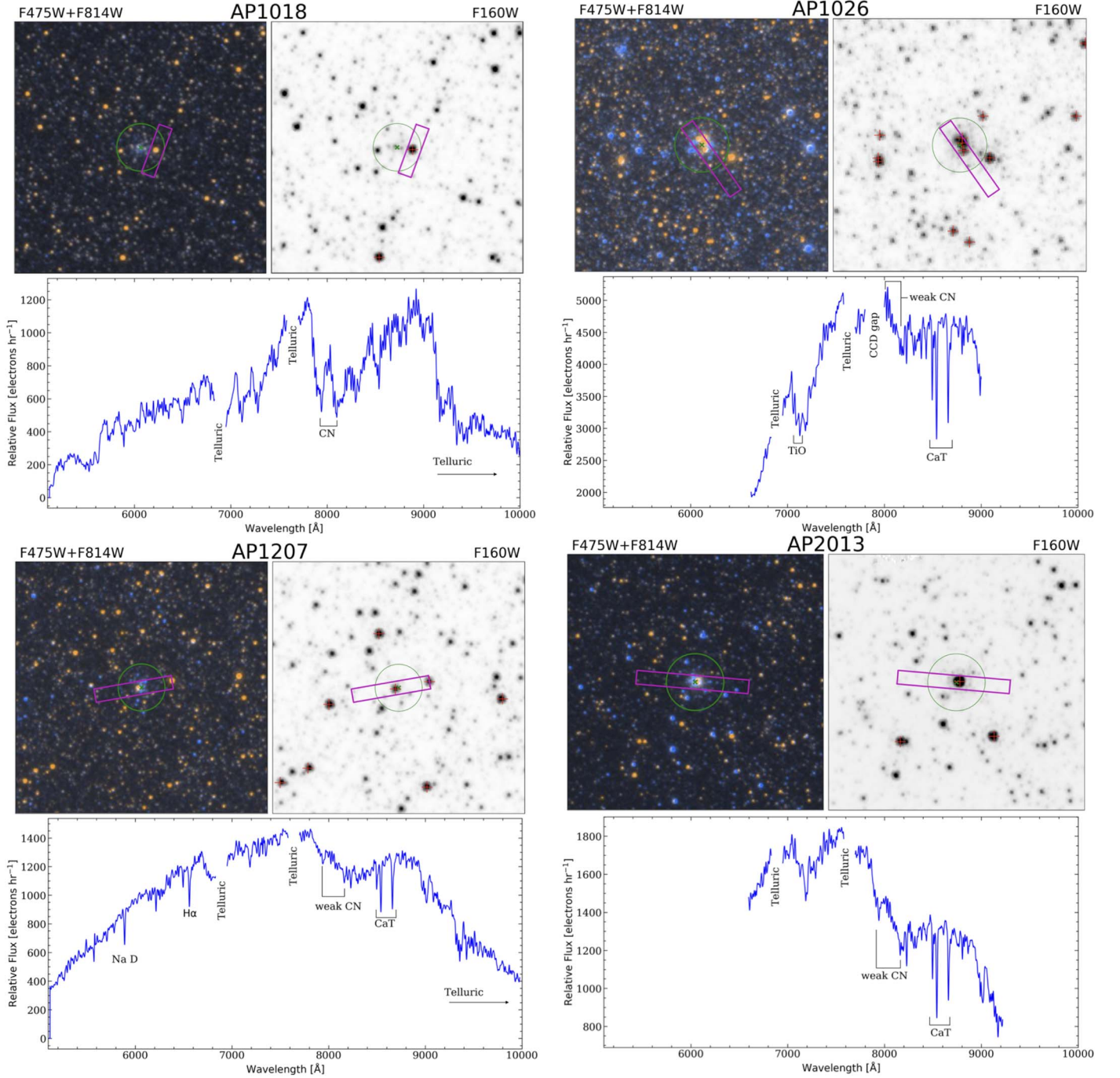
Figure 9. Examples of clusters for which we have spectra from Keck/DEIMOS. To the cluster images and AGB candidate identification in the top panels (as in Figure 4), we add the position of the DEIMOS slit, and the extracted spectrum in the bottom panels. The most prominent spectral features are marked, and the main telluric features are either marked or removed.

mean numbers of AGB candidates per cluster varies between 0 and 0.7.

To proceed in our considerations, we also need to define a "background model," made of stars likely not associated with the clusters, but which are treated in the same way as the stars (real members or not) located in the cluster centers. We define this background model using the AGB candidates located in an annulus with $2R_{\rm ap} < R_{\rm sc} < 4R_{\rm ap}$. This annulus is far enough from the cluster center to be dominated by field stars (see Figure 3), and small enough to not reflect the strong variations

in the field density and mean extinction of star-forming regions in the M31 disk.

5884 candidate AGB stars are found in the $2R_{\rm ap} < R_{\rm sc} < 4R_{\rm ap}$ area around 599 clusters. This sample turns out to present an age distribution clearly different from that of stars inside $R_{\rm ap}$, as shown in the top-right panel of Figure 12. And, not surprisingly, their age–$M_{\rm tot}$ distribution resembles very much the distribution of cluster areas depicted in the bottom-right panel of Figure 11. This indicates that they are indeed sampling the background population of field-AGB
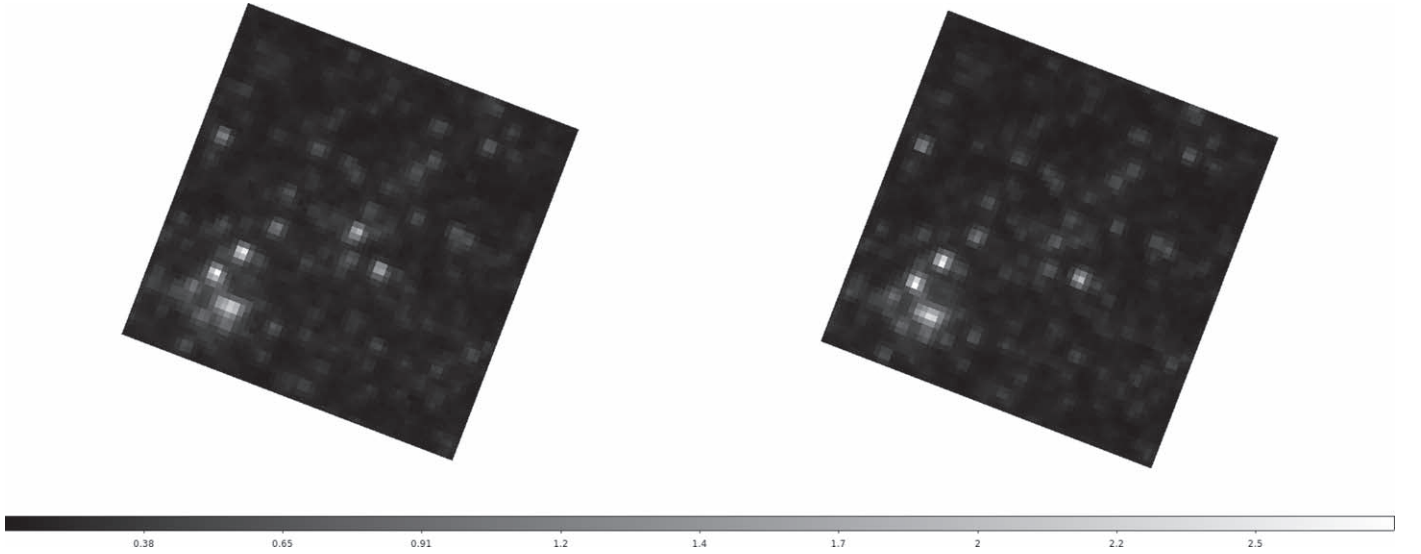
Figure 10. Two images of the AP 2725 cluster in the ACS/WFC F475W filter, taken 201 days apart. The images are centered on the star PHAT10.9645575 +41.500547, which is a candidate AGB star, and whose variation in brightness is evident.

candidates, in proportion to the $12\pi R_{\rm ap}^2$ area around every cluster.

We proceed computing the total F160W luminosity of the candidate AGB stars:

$$L_{\rm AGBc}^{\rm F160W} = \sum_i 10^{-0.4({\rm F160W}_i - 24.50 - 3.37)}, \qquad (5)$$

where 24.50 mag is the adopted distance modulus and 3.37 mag is the solar absolute magnitude in F160W (Willmer 2018). This quantity is computed for both the in-cluster ($R_{\rm sc} < R_{\rm ap}$) and the background ($2R_{\rm ap} < R_{\rm sc} < 4R_{\rm ap}$) samples, and shown in the bottom row of Figure 12.

We finally derive two quantities of direct interest for studies of stellar populations: the numbers of AGB stars and their total luminosities per unit mass of the searched clusters, corrected by the contamination from field stars, for every age bin:

$$\frac{N_{\rm AGBc}}{M_{\rm tot}} = \frac{\sum_i [N_{\rm AGBc,in} - (A_{\rm in}/A_{\rm out}) N_{\rm AGBc,out}]}{\sum_i M_{\rm tot}}, \qquad (6)$$

$$\frac{L_{\rm AGBc}^{\rm F160W}}{M_{\rm tot}} = \frac{\sum_i [L_{\rm AGBc,in}^{\rm F160W} - (A_{\rm in}/A_{\rm out}) L_{\rm AGBc,out}^{\rm F160W}]}{\sum_i M_{\rm tot}}, \qquad (7)$$

where "in" stands for the $R_{\rm sc} < R_{\rm ap}$ region, "out" for the $2R_{\rm ap} < R_{\rm sc} < 4R_{\rm ap}$ annulus, and $A_{\rm in}/A_{\rm out} = 1/12$ for their relative areas. The summations are done over all clusters i inside every age bin, including those without any AGB candidate in their proximity.

All quantities needed to compute Equations (6) and (7) are illustrated in the previous Figures 11 and 12. In particular, $N_{\rm AGBc,in}$ and $L_{\rm AGBc,in}^{\rm F160W}$ are illustrated in the left panels of Figure 12, while $M_{\rm tot}$ is in the top-right panel of Figure 11. The bulk contribution of the background stars to Equations (6) and (7) (i.e., the terms $(A_{\rm in}/A_{\rm out}) N_{\rm AGBc,out}$ and $(A_{\rm in}/A_{\rm out}) L_{\rm AGBc,out}^{\rm F160W}$) in every mass and age bin, can be derived by simply multiplying the numbers in the right panels of Figure 12 by $(1/12)$. In addition, we illustrate in Figure 13 the densities of star counts and of the F160W luminosities in the background sample. These densities differ from a uniform distribution because of the Poisson noise, and possibly also because of the

subtle trends in the distribution of cluster masses and ages as a function of galactocentric distance (hence field density). As can be appreciated, the densities involved in the correction for the background (median values for the entire sample) amount to 0.0223 stars per arcsec^2 and 324 $L_\odot$ per arcsec^2, respectively.

Finally, Figure 14 shows the $N_{\rm AGBc}/M_{\rm tot}$ and $L_{\rm AGBc}^{\rm F160W}/M_{\rm tot}$ curves plotted as a function of age. To derive these curves, we adopt the 0.3 dex wide binning in $\log t$, but move the age bins by small steps of 0.05 dex in $\log t$, so as to avoid producing features that depend on the exact location of the bin boundaries.

In addition, we estimate errors for all the quantities involved. Errors in stars counts are taken as the square root of star counts, while errors in cluster masses and F160W luminosities derive directly from the tabulated values. The final errors follow from the propagation of all errors into $N_{\rm AGBc}/M_{\rm tot}$ and $L_{\rm AGBc}^{\rm F160W}/M_{\rm tot}$, under the assumption that they are independent. Since formal errors in $M_{\rm tot}$ are very small (typically less than 10% per age bin), errors in $N_{\rm AGBc}/M_{\rm tot}$ are dominated by the Poisson noise in $N_{\rm AGBc}$. Errors in $L_{\rm AGBc}^{\rm F160W}/M_{\rm tot}$, instead, turn out to be unrealistically small when computed this way, since they just reflect the tiny errors in measuring the F160W fluxes of several very bright stars. To include the stochastic fluctuations in the number of AGB candidates into this estimate, we assume the fractional error in $L_{\rm AGBc}^{\rm F160W}/M_{\rm tot}$ to be at least as large as the one in $N_{\rm AGBc}/M_{\rm tot}$. These approximated (and possibly underestimated) error bars are also plotted in Figure 14. They should be considered as order-of-magnitude estimates of the random errors, only.

There are other possible errors still not taken into account in the estimates above. For instance, errors related to crowding include a small fraction of AGB candidates ($\sim$55 out of 937) possibly being RGB stars scattered into the AGB region by crowding errors, and the possible blending of a few AGB stars. These errors are not taken into account because they amount to just a few per cent in our present estimates (see Section 2.5), which is much less than the errors caused by the Poisson noise in the values of $N_{\rm AGBc}$. In addition, there are errors associated with the variable AGB stars being observed at random phases of their pulsation cycles. The latter tend to cancel out for large samples, and should be small for the relatively faint AGB stars
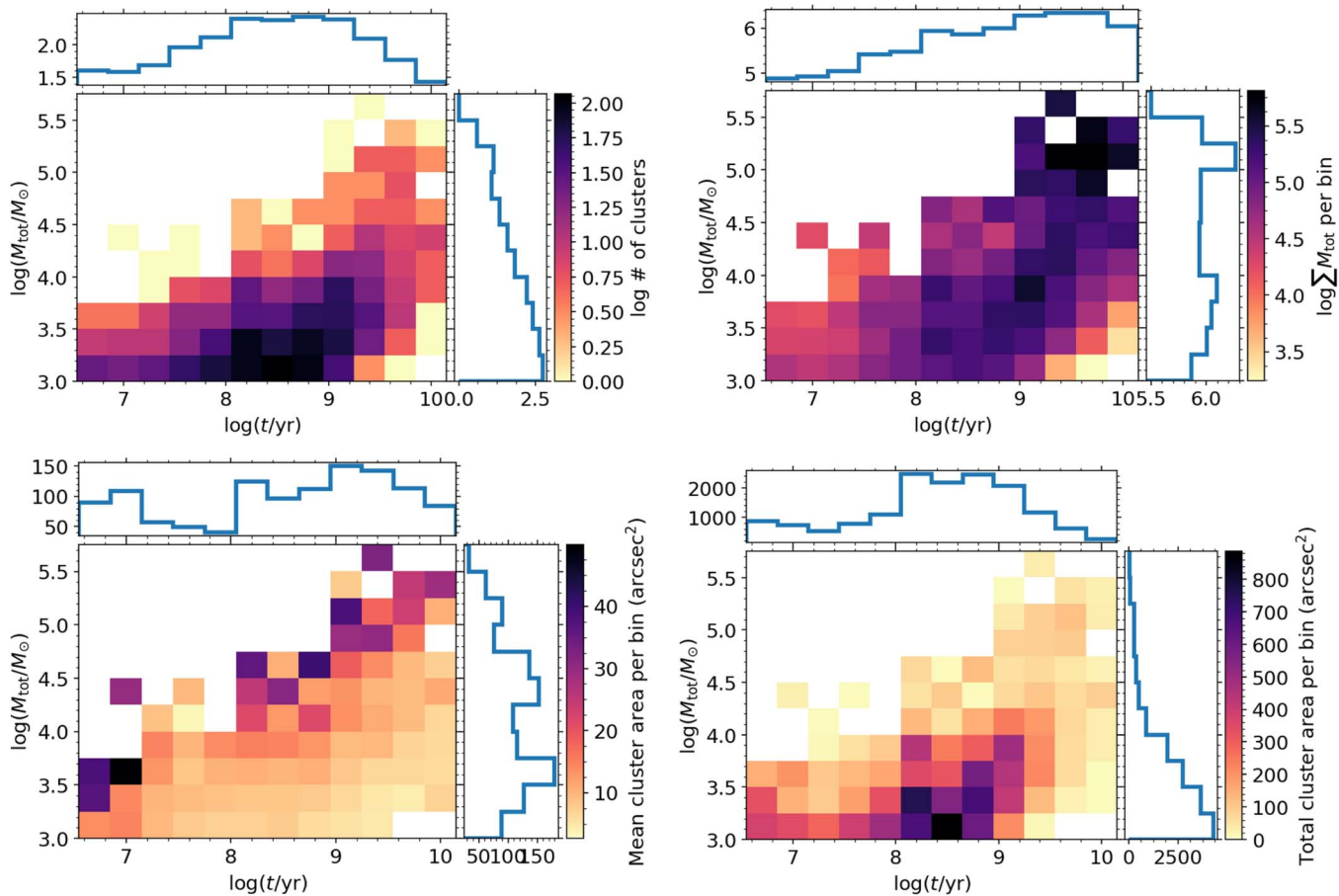
Figure 11. Distribution of the AP cluster data used in this work (not in bulge, with NIR photometry, with ages) on the $\log t$ vs. $\log M_{\rm tot}$ plane. They include all 2736 clusters available, regardless of the presence of AGB candidates. The top-left panel shows the number of clusters per age-mass bin and histograms for both mass and age. The top-right panel shows the same for the total mass comprised in every bin. The bottom-left panel shows the mean area inside $R_{\rm ap}$, for all clusters in a bin. The bottom-right panel shows the total area inside $R_{\rm ap}$ for all clusters in a bin.

located close to the F160W limit of our sample, which are more likely to be low-amplitude pulsators; on the other hand, they might be significant for the brighter and rarer AGB stars that pulsate as large-amplitude Miras. Therefore, the variability effect could be especially affecting our $L_{\rm AGBc}^{\rm F160W}/M_{\rm tot}$ estimates. However, all these errors are not easy to estimate. We believe that a reliable determination of all the errors in Figure 14 can only be reached with a large set of artificial clusters containing variable AGB stars, being inserted into the original PHAT images and having their data recovered exactly as the real clusters.

Finally, one may wonder whether mass segregation between the AGB stars and the other cluster stars that define $R_{\rm ap}$, may be affecting our estimates as well. We consider it unlikely since: (1) in theoretical isochrones (e.g., those by Marigo et al. 2017), AGB stars have initial masses just ~10 % larger that the turn-off stars, which are the less massive stars that can still contribute significantly to the integrated optical light. More-over, (2) most of the mass lost by the presently seen AGB stars was lost in the $\lesssim 2 \times 10^8$ yr time elapsed since their TRGB (or since the beginning of the core-helium burning phase for intermediate-mass and massive stars) stage. These numbers mean too small a mass difference, and too brief a timespan, for significant mass segregation to take place in the relatively small clusters that make the bulk of our sample.

3.3. Comparison with Models

For comparison, in Figure 14 we overplot the same quantities $N_{\rm AGBc}/M_{\rm tot}$ and $L_{\rm AGBc}^{\rm F160W}/M_{\rm tot}$ as derived from the PARSEC-COLIBRI family of isochrones, for initial metalli-cities between $Z_{\rm i} = 0.01$ (slightly below solar, [M/H] = −0.18 dex) and $Z_{\rm i} = 0.017$ (slightly above solar, [M/H] = +0.07 dex), which encompass the median values observed across the M31 disk for galactocentric radii between 4 and 14 kpc (see Gregersen et al. 2015). These models are available online[25] and are described in a series of papers including Bressan et al. (2012), Chen et al. (2015), and Marigo et al. (2017). Their TP-AGB sections result from a major effort to provide models calibrated with observations of resolved stellar populations, as described in Pastorelli et al. (2019, 2020). The quantities $N_{\rm AGBc}/M_{\rm tot}$ and $L_{\rm AGBc}^{\rm F160W}/M_{\rm tot}$ are derived by generating, from the isochrones, the photometry of a population with an initial mass of $M_{\rm tot} = 10^7 M_\odot$, located at a true distance modulus of 24.47 mag and with a foreground extinction of $A_V = 0.17$ mag. Only stars that satisfy our catalog cut (Equations (1) and (2)) are then considered in computing $N_{\rm AGBc}$ and $L_{\rm AGBc}^{\rm F160W}$. No attempt is made to include photometric errors in these simulations.

The $N_{\rm AGBc}/M_{\rm tot}$ quantity is indicative of the product between the lifetimes of AGB stars, $\tau_{\rm AGBc}$, and the rate that stars leave
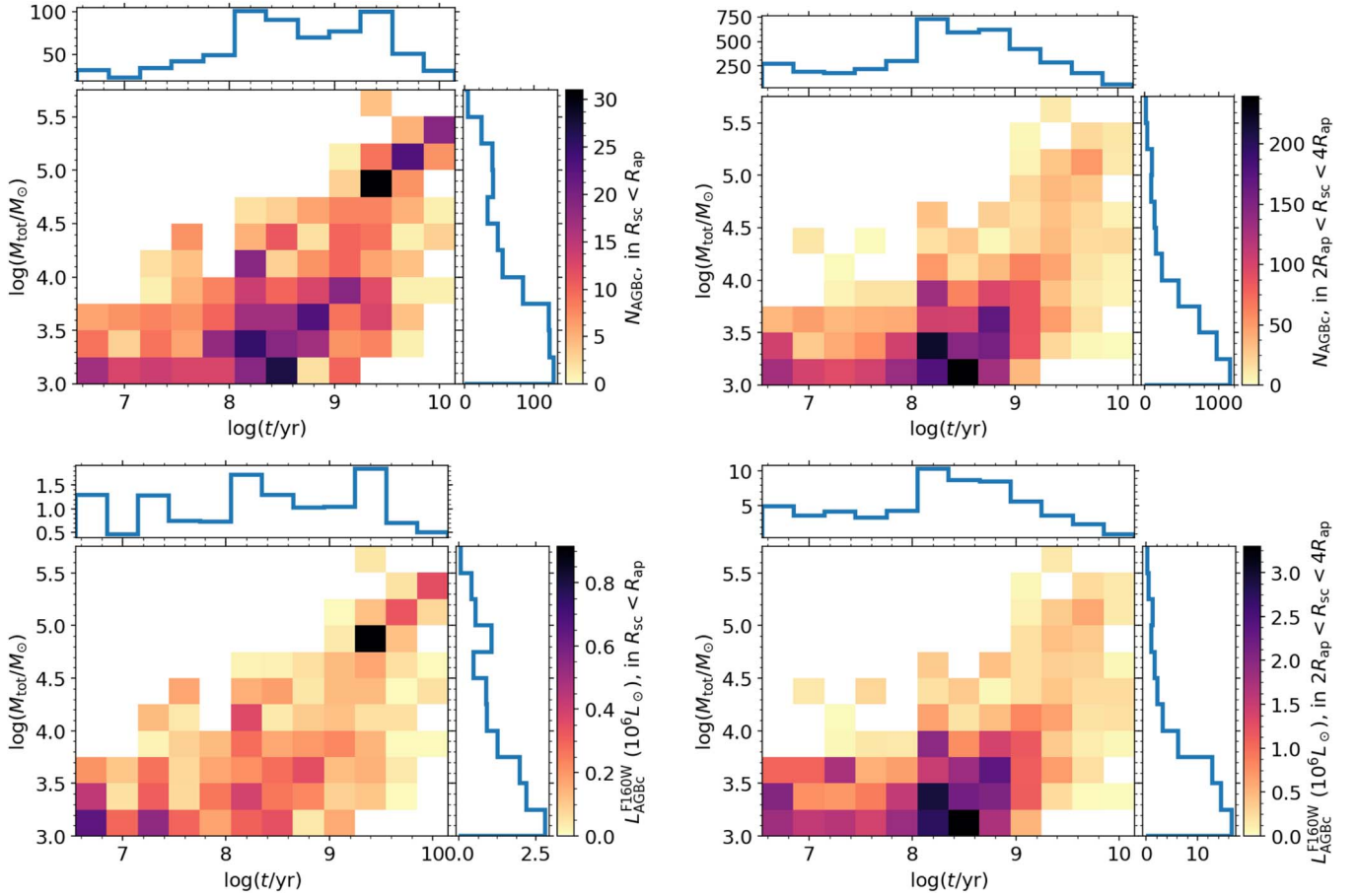
---
[24] http://stev.oapd.inaf.it/cmd

Figure 12. Top row: distribution of the AGB candidates in the $\log t$ vs. $\log M_{tot}$ plane, together with cumulative histograms for both quantities. The top-left panel shows the number of AGB candidates inside the $R_{sc} < R_{ap}$, while the top-right shows the numbers in the "background sample" at $2R_{ap} < R_{sc} < 4R_{ap}$, for which we attribute the same cluster ages and masses as for the stars in $R_{sc} < R_{ap}$. The bottom row shows the same for the total luminosity of these stellar samples in the F160W filter.

the previous evolutionary stages, $b^{AGB}(t)$, as the stellar populations age, that is:

$$\frac{N_{AGBc}}{M_{tot}}(t) \propto \tau_{AGBc}(M_{TO}) \times \phi_{M_{TO}} \times \left| \frac{dt_{eHe}}{dM_i} \right|^{-1}_{M_i = M_{TO}} \quad (8)$$

(see Girardi & Bertelli 1998), where M_{TO} is the turn-off mass corresponding to the age t, $\phi_{M_{TO}}$ is the relative number of these stars as predicted by the initial mass function, and dt_{eHe}/dM_i is the rate at which the stellar age at the end of core He-burning phase changes with the initial mass. In general, all these quantities are well-behaved across very wide intervals of t, with the only exceptions of t_{eHe}, which has a major wiggle at 1.6 Gyr (see Girardi et al. 2013), and of τ_{AGBc} which is expected to vary a lot as a function of both population age and initial mass, as already said. But given this proportionality, the plot of N_{AGBc}/M_{tot} should approach zero at the two extremities of the total age interval, since the lifetimes of all cool giants are expected to be zero for the very young clusters containing only blue and yellow supergiants, and becomes very short again at very old ages, as the AGB phase become short-lived and shifts to sub-TRGB luminosities. This is indeed the case, as can be appreciated in Figure 14. We interpret this result as the consequence of performing a good field subtraction in Equation (6).

Then, the N_{AGBc}/M_{tot} curves present a strong peak at ages $7 < \log(t/yr) < 7.6$. The same peak is evident in the stellar population models. They result from the cool evolutionary stages of massive stars, with masses around $\sim 12M_\odot$, comprising part of the red core-helium burning phase, and the evolution from central He-exhaustion up to C-ignition in the core. Observationally, these stars are usually referred to by the generic name of "RSGs." In the models we plot, their numbers generally increase with increasing metallicity. This increase is mainly the result of the Hayashi line systematically moving to cooler effective temperatures as the metallicity increases, hence moving increasing sections of the isochrones to the red of our color cut at F110W−F160W > 0.88 mag.[25] The comparison in Figure 14 suggests that good agreement between data and models could possibly be obtained at metallicities intermediate between the values $Z_i = 0.01$ and 0.017. However, reproducing this curve is beyond the scope of the present paper, and it would require a careful consideration of the metallicities sampled in the M31 cluster data. From the point of view of the present work, the main conclusion turning out from the comparison is that this peak in the age distribution of cool giants is well explained by the models, but is not related to AGB stars.

The most significant comparison, instead, is for the $8 < \log(t/yr) < 10.1$ age interval, to the right of the vertical gray line, for which the sample is expected to be dominated by
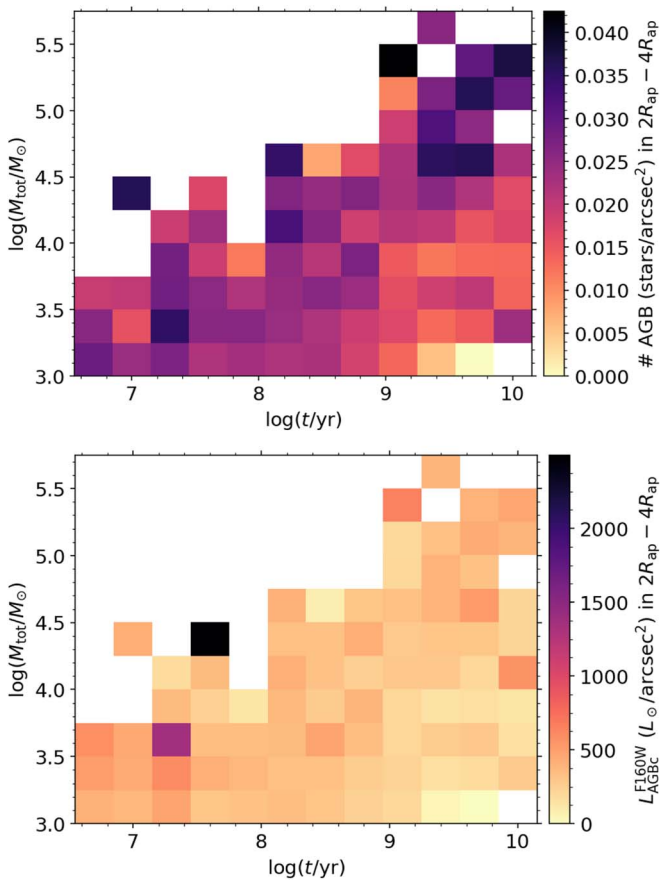
Figure 13. The densities of background field stars contributing to Equations (6) and (7). The top panel is for the number of AGB candidates, the bottom panel is for their total luminosities in the F160W filter.

AGB stars. The $N_{\rm AGBc}/M_{\rm tot}$ curve is observed to decrease almost steadily over this wide age interval, with values going from an initial ~50 stars per million solar masses formed at 10^8 yr, down to just ~5 at very old ages. But this decrease is marked by significant up-and-down jumps over the entire age interval. The most significant of these features is a temporary decrease in the numbers of stars for ages $8.5 < \log(t/{\rm yr}) < 8.8$, where the $N_{\rm AGBc}/M_{\rm tot}$ curve drops from ~40 down to ~20 $\times 10^{-6} M_\odot^{-1}$. Later on, as the curve enters in the regime of very old ages ($\log(t/{\rm yr}) > 10$), it drops again from ~20 down to ~5 $\times 10^{-6} M_\odot^{-1}$. We note that the drop at $8.5 < \log(t/{\rm yr}) < 8.8$ coincides with the transition point between CMD ages from Johnson et al. (2016) and integrated-light ages from Beerman (2015), so we cannot exclude that it reflects some bias in the ages assigned to the sample.

Comparison with the model values indicate that the predicted numbers of AGB stars are in the observed range, considering the error bars, except for a few discrepancies: (1) there is no drop predicted for the star counts in the $8.5 < \log(t/{\rm yr}) < 8.8$ interval, where model values are at least twice larger than the observed ones. In the models, $N_{\rm AGBc}/M_{\rm tot}$ actually presents a peak inside this age interval, which is more evident at sub-solar metallicities. This peak occurs mainly because of a steep increase in the lifetimes of TP-AGB stars, just before their maximum values are reached at $\log(t/{\rm yr}) \simeq 9$ (see also Girardi & Marigo 2007; Marigo et al. 2017; Pastorelli et al. 2019). (2) At ages $9.2 < \log(t/{\rm yr}) < 9.4$, models predict slightly fewer

AGB stars than observed. This age interval corresponds to stars in the TP-AGB phase only, and their numbers present a small dependence on metallicity. It is also the age range in which the "AGB boosting" effect appears in the MC clusters (Girardi et al. 2013). (3) Another discrepancy is evident for the oldest clusters, in the bins at ages $\log(t/{\rm yr}) > 9.5$. Theoretical models of single stars predict very few, if any, AGB stars brighter than the TRGB at these ages, while the data seem to suggest their presence at levels between 20 and $5 \times 10^{-6} M_\odot^{-1}$. The stars observed could be the progeny of close binaries evolved through the blue straggler phase, but their numbers appear definitely too high considering that the most massive globular clusters in the MW present just a handful of blue stragglers, which become much less likely to be observed after evolving into the AGB. Instead, the problem could be in the uncertainties we already mentioned throughout this paper, which become more serious at the limit of old ages. Indeed, the data for old ages depend on a handful of very massive clusters, with $M_{\rm tot} \gtrsim 10^5 M_\odot$ (see top-left panel in Figure 12), including some of the objects which probably have the most serious problems with crowding.

To explore if crowding can really be a serious issue for the oldest clusters, Figure 15 presents the F160W luminosity functions of candidate AGB stars in the clusters, compared to the luminosity function of the background sample, separated in four wide age intervals. As can be noticed, the properties of the background stars are more or less the same in all age bins, and they are concentrated at F160W > 17 mag. For the stars likely to be cluster members (i.e., for the difference between the "in" and "out" histograms in the figure), there is a clear trend of younger age bins having brighter AGB candidates, as expected. They appear as an excess of stars with $16 \lesssim {\rm F160W} \lesssim 17.5$ in the $8 < \log(t/{\rm yr}) < 8.5$ age bin, and as an excess at $16.5 \lesssim {\rm F160W} \lesssim 17.5$ in the $8.5 < \log(t/{\rm yr}) < 9$ age bin. For the oldest age bins, instead, the distributions are clearly concentrated at the faintest luminosities. Although a peak at the faintest magnitudes (F160W $\simeq$ 18 mag) appears for all age bins, this peak is especially remarkable in the oldest age bin, with $\log(t/{\rm yr}) > 9.5$. This serves as a warning that crowding of bright RGB stars could be, for these old clusters, an issue more serious than previously inferred in our previous Section 2.5. Alternatively, we could be witnessing an unexpected excess of AGB stars in M31 old clusters, or very serious errors in their ages.

Finally, the right-hand panel in Figure 14 plots the quantity $L_{\rm AGBc}^{\rm F160W}/M_{\rm tot}$. It is presented here primarily as proxy for the contribution of AGB stars to the NIR light of stellar populations (see e.g., Melbourne et al. 2012). The interpretation of this latter plot is not so obvious. Leaving the discrepancies at very young ages aside, and concentrating on the age interval that corresponds to AGB stars ($\log(t/{\rm yr}) > 8$), we notice the following: first, it is evident that the models reproduce the correct level of $L_{\rm AGBc}^{\rm F160W}/M_{\rm tot}$ in the initial $8.0 < \log(t/{\rm yr}) < 8.5$ interval, but for later ages they either underestimate or overestimate the observed luminosities by factors often in excess of 2. These discrepancies partially reflect the discrepancies already noticed in the $N_{\rm AGBc}/M_{\rm tot}$ plot. The discrepancy seems particularly dramatic as we approach ages $\log(t/{\rm yr}) > 10$—where the model values fall to zero, since no stars above the TRGB are predicted at those ages.

To conclude, we invite the readers to appreciate the general level of agreement between the data and the behavior expected
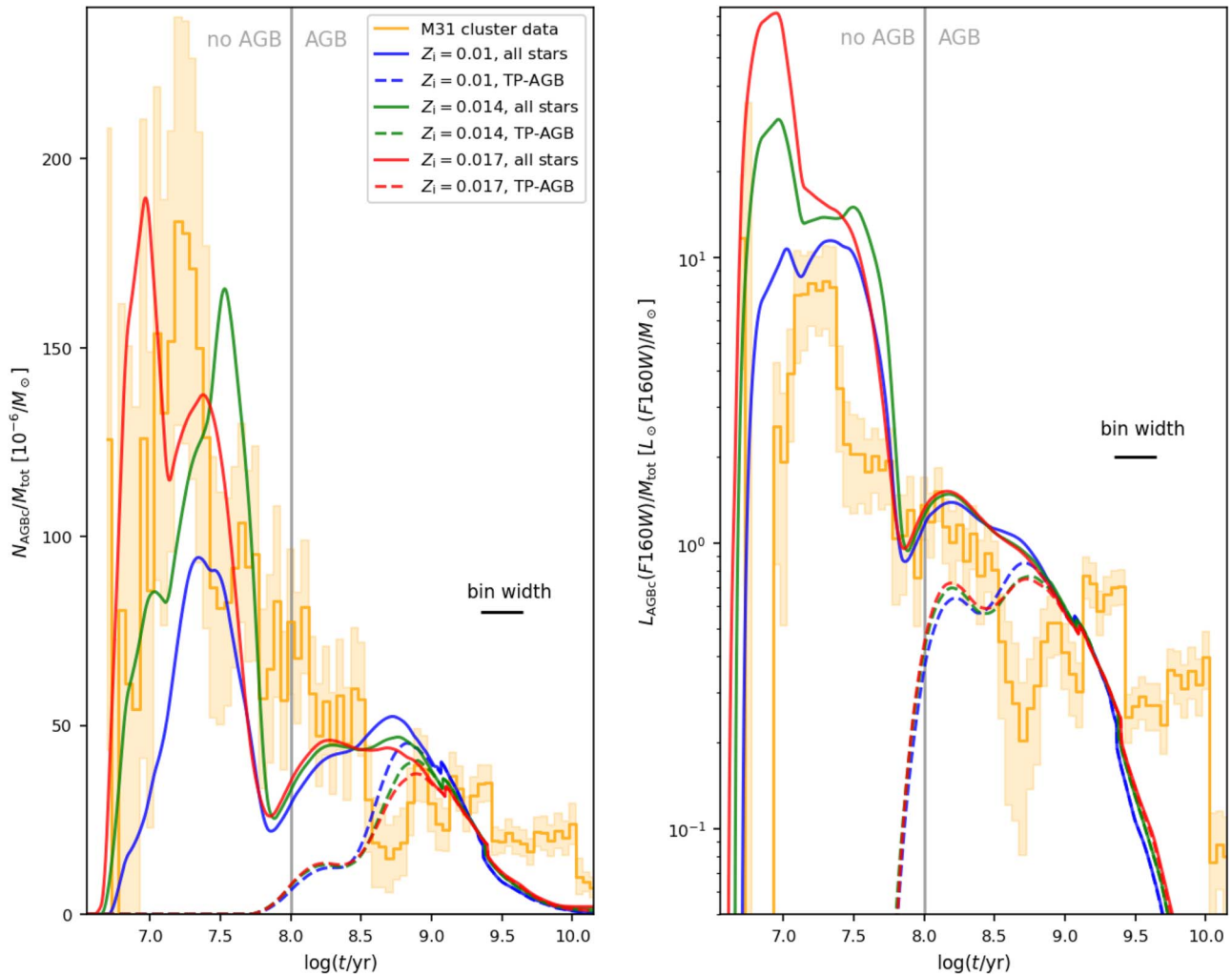
Figure 14. Numbers and luminosities of bright red giants per unit mass of stellar populations, at varying age, as derived from our data and compared to stellar population models. The left panel shows the numbers of AGB candidates observed in every age bin, divided by the total mass of all the clusters in the same bin (orange line). Age bins have a fixed width of 0.3 dex in log(age), and are allowed to move over the interval from very young to very old cluster ages at steps of 0.05 dex. The continuous red, green, and blue lines show the same quantity, derived from the PARSEC-COLIBRI model isochrones, for three values of initial metallicity, and again averaged over 0.3 dex wide age intervals. The dashed lines refer to the stars in the TP-AGB section of the isochrones only. The vertical gray line at $\log(t/\mathrm{yr}) = 8$ separates the broad age ranges where the star counts are expected to be free of AGB stars, and dominated by AGB stars. The right panel shows, for the same data and sets of models, the total stellar luminosity of bright red giants in the F160W filter, relative to the solar luminosity in the same filter, and per unit mass of stellar populations. In both panels, the filled areas indicate the approximate (and probably underestimated) 1σ errors of the data.

from models, over the very wide age interval under consideration, rather than focusing on the localized discrepancies. Given the all sort of limitations we already mentioned—such as the high level of field contamination, the great uncertainties possibly affecting cluster ages and aperture radii, the lack of more extensive simulations of effects of crowding, etc.—this overall agreement was not expected beforehand. It indicates the great potential of these data to offer quantitative constraints to stellar evolution models.

4. Closing Remarks

In this paper, we present a list of candidate AGB stars in M31 star clusters, derived from PHAT NIR photometry added to the AP cluster catalogs built (mainly) from PHAT optical photometry.

The entire data is made available as a High Level Science Product at the MAST.[26] It includes a table with all data used in

this paper, and "finding charts" for all clusters with AGB candidates, as those illustrated in Figures 4–6. The tabulated data comprise all the quantities already described in Williams et al. (2014) for the photometry of individual stars, together with the cluster data from the AP catalog from Johnson et al. (2015), and their age and mass estimates computed as in Fouesneau et al. (2014) and Beerman (2015). To all these data, we add just a few quantities derived in this paper, like the distance of stars from the cluster center (R_{sc}; Section 2.4), a flag to point stars potentially misclassified by crowding, and the RGB density (Section 2.5). We also add the spectral classification (Sections 2.6 and 2.7) and a variability flag (Section 2.8), for the stars for which this information is available.

Out of an initial list of 937 candidates, nearly half (467) are likely field stars appearing by chance within the cluster aperture radius (Section 2). Moreover, out of the 791 candidates with valid cluster ages, 295 belong to clusters that are too young to host an AGB population. These stars are probably not AGB
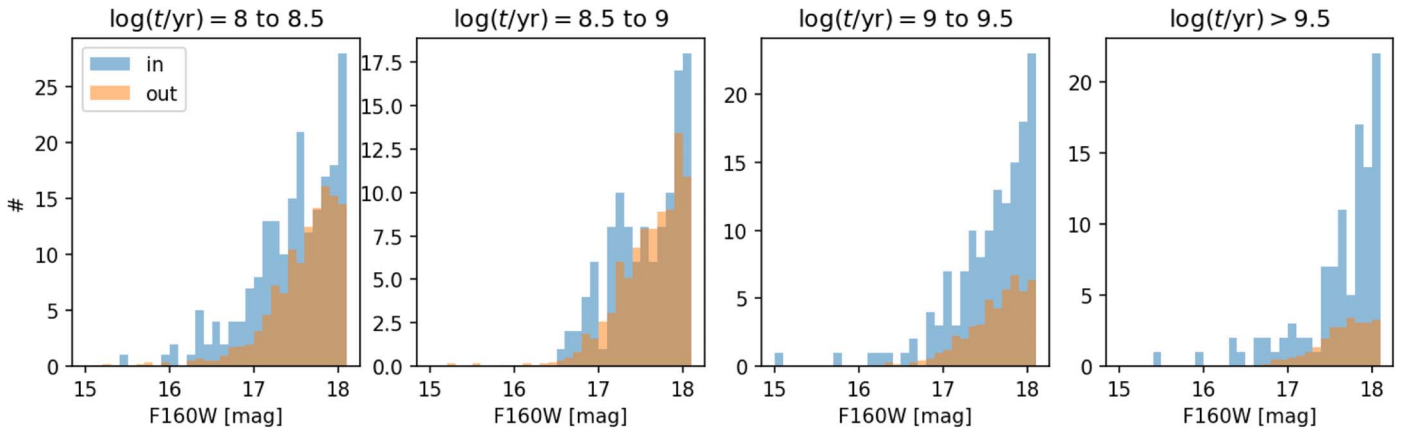
Figure 15. Luminosity functions of AGB candidates ("in," for the sample with $R_{sc} < R_{ap}$), separated in several wide age bins. They are compared to the luminosity functions of the stars effectively used as the background sample ("out," for 1/12 of the luminosity function of the sample with $2R_{ap} < R_{sc} < 4R_{ap}$).

stars but younger "RSGs" of different kinds (Section 3). Taking these fractions into consideration, our catalog contains ∼294 stars which are very likely AGB members of star clusters in M31. This number exceeds by a factor of ∼2 any other list of AGB stars in clusters, including those for the MCs which have driven so much progress in our understanding of this evolutionary phase.

Therefore, the present sample of candidate AGB stars might be a treasure trove for future studies of stellar evolution. For instance, they might help to set clearer constraints on the mass and age intervals that allow for the formation of C and S stars, and their luminosities, and allow a more direct assessment of their evolutionary lifetimes. These constraints are badly needed at the high metallicities that characterize M31 and the MW galaxy. Similar studies in the MW clusters do not appear that promising, given the small samples of stellar clusters available in optical surveys (from where ages are better determined), and their small masses. Although Gaia, the Rubin Observatory Legacy Survey of Space and Time, and future wide-area high-resolution NIR surveys (e.g., with the Nancy Grace Roman Space Telescope) might improve this situation, having a sample of clusters observed from outside, and with a good understanding of their contaminating foreground/background like in M31, will certainly help.

Many of the population studies enabled by the present catalog will, however, require follow-up observations of some kind, and more evidently: (1) spectroscopy to determine the spectral types of the TP-AGB candidates (broadly speaking, into M, C, S, dust-obscured, and CN-weak subtypes, see e.g., Hamren et al. (2015) and the examples in Section 2.7), and hopefully their radial velocities compared to the clusters for membership probabilities; or alternatively (2) narrow/medium-band photometry for a more efficient C/M classification (see Boyer et al. 2013, 2019, and Section 2.6); (3) time series photometry to identify long-period variables (as in Section 2.8) and to determine their pulsation periods and modes, either with adaptive optics or with future space-based NIR facilities like the James Webb and Roman space telescopes; (4) higher resolution, deeper optical photometry for improving cluster age determinations. The present catalogs are released especially to motivate such follow-up efforts.

However, it is also clear that the M31 sample, as a whole, will be much more affected by the problems of field contamination and age uncertainties than the AGB star samples already studied in the MCs clusters. They will therefore require careful analysis of membership probabilities and simulations of measurement errors in the stellar photometry, and in the cluster ages and masses. These aspects will be more thoroughly discussed in a forthcoming paper, where the M31 sample will be compared with a similar sample from M33 (HST-GO-14610, PI: Dalcanton).

Facilities: HST (ACS), HST (WFC3), Keck (DEIMOS).

Software: Perl (Wall et al. 2000), STILTS (Taylor et al. 2006), astropy (Astropy Collaboration et al. 2013), DOLPHOT (Dolphin 2016).

ORCID iDs

Léo Girardi ⓘ https://orcid.org/0000-0002-6301-3269
Martha L. Boyer ⓘ https://orcid.org/0000-0003-4850-9589
L. Clifton Johnson ⓘ https://orcid.org/0000-0001-6421-0953
Julianne J. Dalcanton ⓘ https://orcid.org/0000-0002-1264-2006
Philip Rosenfield ⓘ https://orcid.org/0000-0001-9306-6049
Anil C. Seth ⓘ https://orcid.org/0000-0003-0248-5470
Evan D. Skillman ⓘ https://orcid.org/0000-0003-0605-8732
Daniel R. Weisz ⓘ https://orcid.org/0000-0002-6442-6030
Benjamin F. Williams ⓘ https://orcid.org/0000-0002-7502-0597
Antara Raaghavi Bhattacharya ⓘ https://orcid.org/0000-0002-4342-4626
Alessandro Bressan ⓘ https://orcid.org/0000-0002-7922-8440
Nelson Caldwell ⓘ https://orcid.org/0000-0003-2352-3202
Yang Chen ⓘ https://orcid.org/0000-0002-3759-1487
Andrew E. Dolphin ⓘ https://orcid.org/0000-0001-8416-4093
Morgan Fouesneau ⓘ https://orcid.org/0000-0001-9256-5516
Steven Goldman ⓘ https://orcid.org/0000-0002-8937-3844
Puragra Guhathakurta ⓘ https://orcid.org/0000-0001-8867-4234

Paola Marigo ● https://orcid.org/0000-0002-9137-0773
Sagnick Mukherjee ● https://orcid.org/0000-0003-1622-1302
Giada Pastorelli ● https://orcid.org/0000-0002-9300-7409
Amanda Quirk ● https://orcid.org/0000-0001-8481-2660
Monika Soraisam ● https://orcid.org/0000-0001-6360-992X
Michele Trabucchi ● https://orcid.org/0000-0002-1429-2388

References

Astropy Collaboration, Robitaille, T. P., Tollerud, E. J., et al. 2013, A&A, 558, A33

Beerman, L. C. 2015, PhD thesis, Univ. of Washington

Bernard, E. J., Ferguson, A. M. N., Barker, M. K., et al. 2012, MNRAS, 420, 2625

Bernard, E. J., Ferguson, A. M. N., Chapman, S. C., et al. 2015, MNRAS, 453, L113

Boyer, M. L., Girardi, L., Marigo, P., et al. 2013, ApJ, 774, 83

Boyer, M. L., McDonald, I., Loon, J. T., et al. 2008, AJ, 135, 1395

Boyer, M. L., Srinivasan, S., van Loon, J. T., et al. 2011, AJ, 142, 103

Boyer, M. L., van Loon, J. T., McDonald, I., et al. 2010, ApJL, 711, L99

Boyer, M. L., Williams, B. F., Aringer, B., et al. 2019, ApJ, 879, 109

Bressan, A., Marigo, P., Girardi, L., et al. 2012, MNRAS, 427, 127

Brown, T. M., Smith, E., Ferguson, H. C., et al. 2006, ApJ, 652, 323

Caldwell, N., Harding, P., Morrison, H., et al. 2009, AJ, 137, 94

Catchpole, R. M., & Feast, M. W. 1973, MNRAS, 164, 11P

Chen, Y., Bressan, A., Girardi, L., et al. 2015, MNRAS, 452, 1068

Cioni, M.-R. L., Clementini, G., Girardi, L., et al. 2011, A&A, 527, A116

Cioni, M.-R. L., Girardi, L., Marigo, P., & Habing, H. J. 2006a, A&A, 448, 77

Cioni, M.-R. L., Girardi, L., Marigo, P., & Habing, H. J. 2006b, A&A, 452, 195

Dalcanton, J. J., Williams, B. F., Lang, D., et al. 2012, ApJS, 200, 18

Davidge, T. J. 2012, ApJL, 749, L7

Davis, B. D., Bond, H. E., Ciardullo, R., & Jacoby, G. H. 2019, ApJ, 884, 115

Dolphin, A. 2016, DOLPHOT: Stellar Photometry, Astrophysics Source Code Library, ascl:1608.013

Dorman, C. E., Guhathakurta, P., Fardal, M. A., et al. 2012, ApJ, 752, 147

Dorman, C. E., Guhathakurta, P., Seth, A. C., et al. 2015, ApJ, 803, 24

Dorman, C. E., Widrow, L. M., Guhathakurta, P., et al. 2013, ApJ, 779, 103

Ferguson, A. M. N., Johnson, R. A., Faria, D. C., et al. 2005, ApJL, 622, L109

Ferraro, F. R., Messineo, M., Fusi Pecci, F., et al. 1999, AJ, 118, 1738

Fouesneau, M., Johnson, L. C., Weisz, D. R., et al. 2014, ApJ, 786, 117

Frogel, J. A., Mould, J., & Blanco, V. M. 1990, ApJ, 352, 96

Galleti, S., Federici, L., Bellazzini, M., Fusi Pecci, F., & Macrina, S. 2004, A&A, 416, 917

Gaustad, J. E., & Conti, P. S. 1971, PASP, 83, 351

Gilbert, K. M., Guhathakurta, P., Kalirai, J. S., et al. 2006, ApJ, 652, 1188

Girardi, L., & Bertelli, G. 1998, MNRAS, 300, 533

Girardi, L., & Marigo, P. 2007, A&A, 462, 237

Girardi, L., Marigo, P., Bressan, A., & Rosenfield, P. 2013, ApJ, 777, 142

Gregersen, D., Seth, A. C., Williams, B. F., et al. 2015, AJ, 150, 189

Guhathakurta, P., Ostheimer, J. C., Gilbert, K. M., et al. 2005, arXiv:astro-ph/0502366

Guhathakurta, P., Rich, R. M., Reitzel, D. B., et al. 2006, AJ, 131, 2497

Hamren, K. M., Rockosi, C. M., Guhathakurta, P., et al. 2015, ApJ, 810, 60

Hartwick, F. D. A., & Hesser, J. E. 1973, ApJ, 183, 883

Herwig, F. 2005, ARA&A, 43, 435

Höfner, S., & Olofsson, H. 2018, A&ARv, 26, 1

Javadi, A., van Loon, J. T., & Mirtorabi, M. T. 2011, MNRAS, 414, 3394

Johnson, L. C., Seth, A. C., Dalcanton, J. J., et al. 2012, ApJ, 752, 95

Johnson, L. C., Seth, A. C., Dalcanton, J. J., et al. 2015, ApJ, 802, 127

Johnson, L. C., Seth, A. C., & Dalcanton, J. J. 2016, ApJ, 827, 33

Kalinowski, J. K., Burkhead, M. S., & Honeycutt, R. K. 1974, ApJL, 193, L77

Kamath, D., Karakas, A. I., & Wood, P. R. 2012, ApJ, 746, 20

Kamath, D., Wood, P. R., Soszyński, I., & Lebzelter, T. 2010, MNRAS, 408, 522

Lattanzio, J. C., & Wood, P. R. 2004, Evolution, Nucleosynthesis, and Pulsation of AGB Stars (New York: Springer), 23

Lebzelter, T., Lederer, M. T., Cristallo, S., et al. 2008, A&A, 486, 511

Lebzelter, T., Nowotny, W., Hinkle, K. H., Höfner, S., & Aringer, B. 2014, A&A, 567, A143

Lebzelter, T., & Wood, P. R. 2005, A&A, 441, 1117

Lebzelter, T., & Wood, P. R. 2011, A&A, 529, A137

Lewis, A. R., Dolphin, A. E., Dalcanton, J. J., et al. 2015, ApJ, 805, 183

Maraston, C. 2005, MNRAS, 362, 799

Marigo, P., & Girardi, L. 2007, A&A, 469, 239

Marigo, P., Girardi, L., Bressan, A., et al. 2017, ApJ, 835, 77

Marigo, P., Girardi, L., & Chiosi, C. 1996, A&A, 316, L1

McDonald, I., Boyer, M. L., van Loon, J. T., & Zijlstra, A. A. 2011a, ApJ, 730, 71

McDonald, I., van Loon, J. T., Decin, L., et al. 2009, MNRAS, 394, 831

McDonald, I., van Loon, J. T., Sloan, G. C., et al. 2011b, MNRAS, 417, 20

Melbourne, J., Williams, B. F., Dalcanton, J. J., et al. 2012, ApJ, 748, 47

Momany, Y., Saviane, I., Smette, A., et al. 2012, A&A, 537, A2

Noël, N. E. D., Greggio, L., Renzini, A., Carollo, C. M., & Maraston, C. 2013, ApJ, 772, 58

Pastorelli, G., Marigo, P., Girardi, L., et al. 2019, MNRAS, 485, 5666

Pastorelli, G., Marigo, P., & Girardi, L. 2020, MNRAS, tmp, 2478

Peacock, M. B., Maccarone, T. J., Knigge, C., et al. 2010, MNRAS, 402, 803

Pessev, P. M., Goudfrooij, P., Puzia, T. H., & Chandar, R. 2008, MNRAS, 385, 1535

Quirk, A., Guhathakurta, P., Chemin, L., et al. 2019, ApJ, 871, 11

San Roman, I., Sarajedini, A., & Aparicio, A. 2010, ApJ, 720, 1674

Santos, J. F. C., Jr., & Frogel, J. A. 1997, ApJ, 479, 764

Sarajedini, A., & Mancone, C. L. 2007, AJ, 134, 447

Schweizer, F., Miller, B. W., Whitmore, B. C., & Fall, S. M. 1996, AJ, 112, 1839

Senchyna, P., Johnson, L. C., Dalcanton, J. J., et al. 2015, ApJ, 813, 31

Soraisam, M. D., Bildsten, L., Drout, M. R., et al. 2020, ApJ, 893, 11

Taylor, M. B. 2006, in ASP Conf. Ser. 351, Astronomical Data Analysis Software and Systems XV, ed. C. Gabriel et al. (San Francisco, CA: ASP), 666

van Loon, J. T., Marshall, J. R., & Zijlstra, A. A. 2005, A&A, 442, 597

Wall, L., Christiansen, T., Orwant, J., et al. 2000, Programming perl, (Sebastopol, CA: O'Reilly Media)

Whitmore, B. C., Zhang, Q., Leitherer, C., et al. 1999, AJ, 118, 1551

Williams, B. F., Dolphin, A. E., Dalcanton, J. J., et al. 2017, ApJ, 846, 145

Williams, B. F., & Hodge, P. W. 2001, ApJ, 548, 190

Williams, B. F., Lang, D., Dalcanton, J. J., et al. 2014, ApJS, 215, 9

Willmer, C. N. A. 2018, ApJS, 236, 47